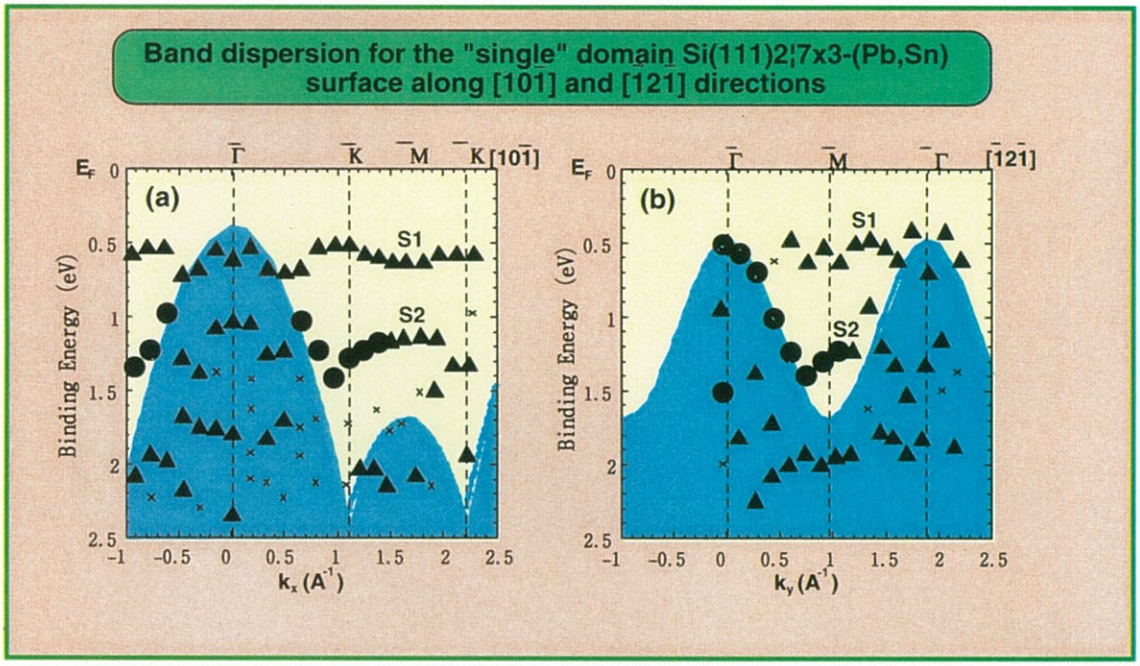

Solid State Spectroscopy Ⅱ

(XAFS, PES)

BL1A, 2B1, 5A, 5B, 6A2, 7A, 8B1, 8B2

parallel to the molecular plane at C=O parts) was not resolved after the In deposition, while new band X' (E_B = ~ 3.6eV) is observed at θ = ~ 62° . These spectral changes originate from a chemical reaction between the PTCDA molecules and the In atoms. The disappearance of the $n_{O\parallel}$ band in Fig.1(b) suggests that the chemical reaction between PTCDA and In takes place at the C=O parts to change the $n_{O\parallel}$ states. It is expected the band X' originates from the molecular orbital which is distributed parallel to the surface, since the band X' observed at a large value of θ.

On the other hand, we performed Penning ionization electron spectroscopy of the In/PTCDA interface. The result suggested that four In atoms react with the one PTCDA molecule.[4]

In Fig.2, we compared the observed ARUPS of the In/PTCDA with the results of *ab initio* MO calculation (STO-6G) on an expected model compound of the reaction product, In_4PTCDA. In Fig.2 θ-averaged spectrum is shown. From the calculation we found that band 1 consists of a single MO of π character with large contribution from C 2pz, O 2pz, and In 5pz atomic orbitals (AOs). On the other hand, the band 3 is related to four σ MOs with the contributions of O 2s, In 5s, 5px, and 5py AOs. The calculated density-of-states (DOS) curve agrees well with the measured ARUPS, indicating that the X and X' are assigned to the π and σ orbitals of In_4PTCDA, respectively. The agreement indicates that the electronic structure of the In/PTCDA is well simulated by that of the model compound In_4PTCDA.

In Fig.3, the observed θ dependence of the band X intensity is compared with the calculated one for molecular tilt angle of β = 0°, 10°, and 20° using the SS/MO method. Among these, the calculated θ pattern for β = 10° agrees better with the observed one in the value of θ_{max} and the width of the angular distribution. The calculated θ dependence for various β with a long molecular axis parallel to the surface showed remarkable disagreement from the observed results. These results indicate that molecules become tilted by the reaction, and the averaged tilt angle is considered to be approximately 10° as shown in Fig.3.

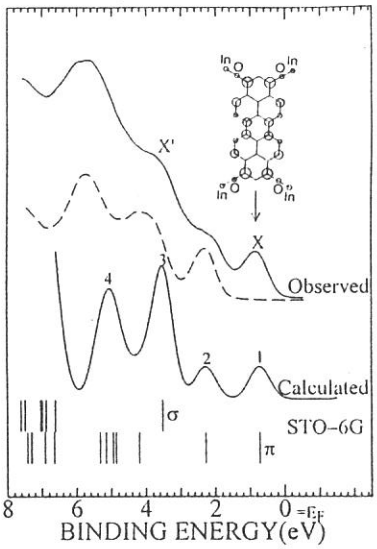

Figure 2 Comparison between observed UPS and the DOS calculated for a model system of the reaction product, In_4PTCDA. The vertical bars show the calculated MO levels. The upper and lower bars indicate σ and π states respectively. The calculated DOS was obtained by a Gaussain broadening of the MO levels. The observed ARUPS's of the pristine PTCDA (– – – – –) and the In/PTCDA (————) are shown for comparison. The molecular orbital coefficients of the π-band X in the reacted system are shown schematically.

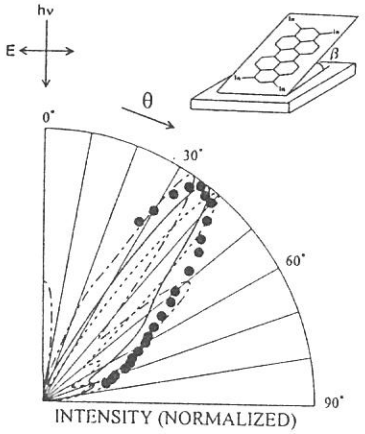

Figure 3 Comparison between calculated and observed θ dependencies of the photoelectron intensities for the band gap state. The SS/MO results at hν=40eV and α=0° are shown for β=0° (– – – – –), 10° (————), and 20° (- - - - - - - - - -). The calculation was made by assuming azimuthal disorder of the reaction product, In_4PTCDA. The tilt direction of the molecule is also shown.

REFERENCES

[1]Y.Hirose, A.Kahn, V.Aristov, P.Soukiassian, V.Bulovic, and S.R.Forrest, Phys. Rev. B 54. 13748(1996).

[2]N.Ueno *et al.*, J.Chem.Phys. **107**, 2079 (1997).

[3]Y.Azuma *et al.*, J. Synchrotron Radiation **5**, 1044 (1998).

[4] S.Kera *et al.*, to be published.

(BL8B1)

Faraday Rotation Measurement on a Co film around $M_{2,3}$ Edges

K. Saito, W. Hu, T. Hatano, T. Ejima and M. Watanabe
Research Institute for Scientific Measurements, Tohoku University
Katahira 2-1-1, Aoba-ku, Sendai 980-8577

We had developed a polarimeter which enables Faraday rotation measurements in the 55-90 eV region by the use of Al/YB_6 multilayer polarizers[1]. It consists of a transmission multilayer polarizer, a magnetic circuit composed of Sm-Co permanent magnets and a rotating analyzer unit consisting of a reflection multilayer analyzer, a multi-channel plate and a pulse motor. In our previous experiment on Ni films around $M_{2,3}$ edges[2], the Faraday rotation angles obtained by using the polarimeter were larger than those calculated from MCD spectrum measured by the total photoelectron yield (TY) method[3], through Kramers-Krönig analysis. It was concluded that the Faraday rotation measurements are transmission measurements, so that they are scarcely affected by surface conditions and reflect bulk properties.

In this experiment, the Faraday rotation measurement on a 21 nm Co film has been performed around $M_{2,3}$ edges under an applied magnetic field of 0.82 T at room temperature. Figure 1 shows the preliminary result of the Faraday rotation spectrum obtained by the present experiment and the calculated one from MCD spectrum measured by the TY method, through Kramers-Krönig analysis. The former spectrum is similar to the latter one. However, the measurement of MCD was performed under a magnetic field of 1.2 T at 140 K (the saturation magnetic field of Co : 1.8 T), so that the absolute value calculated from MCD should be larger than the present result. This means that the MCD measurement was affected by the surface condition and the Faraday rotation measurement reflects bulk properties well as in the case of Ni. However, it is necessary to carry out additional experiments to confirm this conclusion.

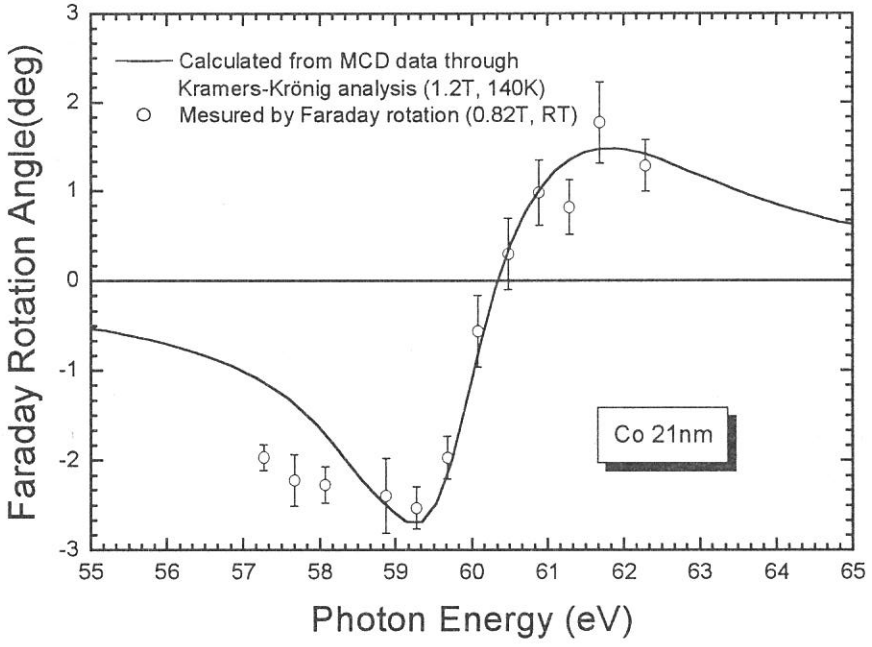

Fig. 1. Faraday rotation spectra of Co around $M_{2,3}$ edges.

References

1) W. Hu, T. Hatano, M. Yamamoto and M. Watanabe, J. Synch. Rad. **5** (1998) 732.
2) T. Hatano, W. Hu, K. Saito, M. Watanabe, J. Electr. Spectr. Rel. Phenom. **101-103** (1999) 287.
3) T. Hatano, S.Y. Park, T. Hanyu, T. Miyahara, J. Electr. Spectr. Rel. Phenom. **78** (1996) 217.

(BL1A)

Mg and Al K-Edge XAFS Measurements with a KTP Crystal Monochromator

Yasutaka Takata and Nobuhiro Kosugi

Institute for Molecular Science,
Myodaiji, Okazaki 444-8585

There has been a strong demand for the monochromator crystals with a large lattice spacing in order to measure the EXAFS spectra for Mg and Al K-edges. At BL1A, beryl ($10\bar{1}0$) [2d=15.965Å] and quartz ($10\bar{1}0$) [2d=8.512Å] are used as the crystal monochromator for the Mg and Al K-edge X-ray absorption fine structure (XAFS) spectra, respectively, and serve soft X-rays with high quality in the near edge region. However, the energy range (k range) is limited because beryl and quartz contain Al and Si, respectively. In the EXAFS analysis, the reliability and accuracy depend strongly on the k range. At the XAFS-X conference (Chicago, 1998), Rogalev et al. reported that KTP, $KTiOPO_4$, (011) [2d=10.95Å] crystal can be used in the crystal monochromator at the ESRF ID12A beamline (circularly polarized undulator) [1]. We have introduced KTP crystal (Crystal Laser Co., France) at BL1A and tested the performance in the energy range below 2100eV including the applicability to the EXAFS measurements for Al and Mg K-edges.

Figure 1 shows the throughput spectra of the KTP double crystal monochromator. The solid line indicates the photon flux measured by the Si photodiode (IRD Co.). The Si K-edge jump at around 1840 eV originates from the photodiode. The total electron yield spectrum of Au plate (broken line) is also shown as a reference. It should be noticed that there is no structure up to 2140eV (P K-edge). On the other hand, YB_{66} (400) [2d=11.72Å] crystal monochromator covering the same energy range shows undesirable structures at around 1400eV due to the anomalous (600) reflection [2-4]. Furthermore, as pointed out by Rogalev et al., the reflectivity of KTP was higher than that of YB_{66}. The energy width of the monochromatized beam was 0.5~0.6 eV in the energy range from 1200 to 2100 eV. We must mention about the radiation damage of the KTP crystal. At the ESRF ID12A, the damage was not noticeable: on the other hand, the present first crystal suffered the damage at BL1A similarly to the case of beryl and quartz crystals. Fortunately, the damage was not so serious and we could measure the EXAFS spectra.

Figure 2 and 3 shows the Mg and Al K-edge XAFS spectra of MgO and α-Al_2O_3, respectively, measured by monitoring the sample drain current. These samples are powder and spread on adhesive conduction tapes. For both spectra, the energy range is extended considerably in comparison with the spectra measured with the beryl and quartz monochromator. In the latter cases, Mg and Al K-edge XAFS spectra are limited up to 1560 eV (Al K-edge) and 1840 eV (Si K-edge).

References

[1] A. Rogalev et al., Abstract of XAFS X, (1998) R5.1-20.
[2] M. Rowen et al., Synchrotron Rad. News, **6** (1993) 25.
[3] T. Tanaka et al., J. Appl. Cryst., **30** (1997) 87.
[4] A. D. Smith et al., J. Synchrotron Rad., **5** (1998) 716.

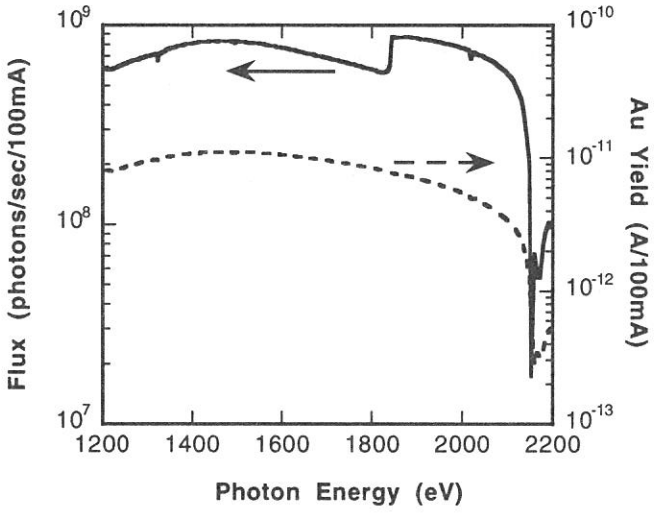

Figure 1. Throughput spectra of the KTP double crystal monochromator at BL1A.

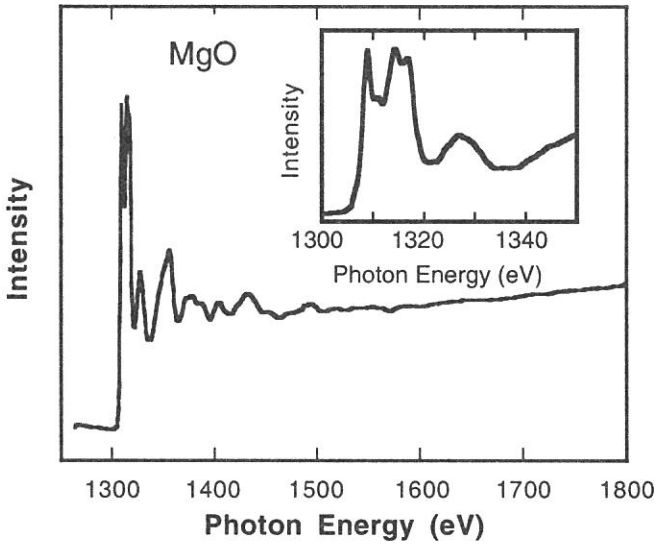

Figure 2. A Mg K-edge XAFS spectrum of MgO.

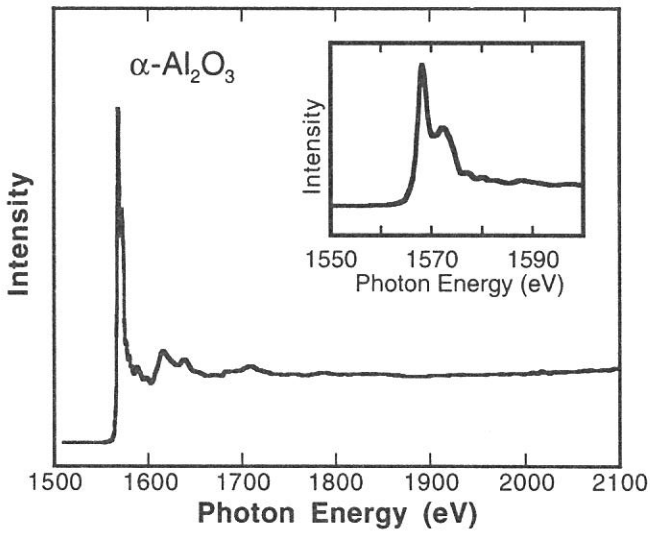

Figure 3. An Al K-edge XAFS specrum of α-Al_2O_3.

(BL1A)

Ni 2p Photoabsorption and Resonant Photoionization of Ni(*NN'*-dimethylethylenediamine)$_2$Cl$_2$

Yasutaka Takata, Takaki Hatsui and Nobuhiro Kosugi

Institute for Molecular Science,
Myodaiji, Okazaki 444-8585

We have reported that the planar Ni complexes with a $3d^8$ low-spin ground state show distinct satellite structures in the Ni 2p photoabsorption spectra [1, 2], and show characteristic resonant behavior in the Ni 3p and 3s resonant photoelectron spectra in comparison with Ni metal and NiO [3-5]. The observed characteristics can be interpreted within a one electron picture taking the ligand vacant orbitals into account. In the present study, we have measured Ni 2p photoabsorption and resonant photoelectron spectra of Ni(*NN'*-dimethylethylenediamine: DED)$_2$Cl$_2$ with a $3d^8$ high-spin state in order to investigate how the spin state influences the spectra.

Experiments were performed at BL1A soft x-ray beamline. A pair of beryl $(10\bar{1}0)$ crystals was used in the double crystal monochromator. The Ni(DED)$_2$Cl$_2$ powder was spread on an adhesive conduction tape. The Ni 2p photoabsorption spectra were measured by monitoring the total electron yield. A SCIENTA SES200 electron energy analyzer was used to measure the photoelectron spectra. The total energy resolution in the photoelectron spectra was about 0.7 eV.

The Ni 2p photoabsorption spectrum of Ni(DED)$_2$Cl$_2$ (Fig.1) shows two strong peaks at the $2p_{3/2}$ edge, and is quite similar to the spectrum of Ni(cyclam)Cl$_2$ [6]. In Ni(DED)$_2$Cl$_2$, Ni is in a D_{4h} symmetry with the apical Cl atoms. The spectrum is quite different from the planar Ni complexes with a $3d^8$ low-spin ground state such as $K_2Ni(CN)_4H_2O$ [1]and Ni(Hdmg)$_2$ [2].

Figure 2 shows the resonant photoelectron spectra in the Ni 3p and 3s ionization regions measured at the excitation energies (0-3) marked in Fig. 1. The intensity was normalized referring that of the Cl 2p photoelectron peaks which are independent of the resonant condition. In the non-resonant spectrum (0), strong satellite bands appear, and are strongly enhanced by the resonant excitation. All the enhanced satellite bands in the spectra (1-3) have constant binding energies, and no noticeable binding energy shift was observed; i.e., there is no clear relation between the photoexcited states and the resonantly enhanced satellite states. These results are similar to those for NiO [3], in which the correlation and multiplet interaction are very important, but are quite different from those for the low-spin planar complexes. In $K_2Ni(CN)_4$[3, 4]and Ni(Hdmg)$_2$[5] weak or hidden satellite bands in the non-resonant spectra are enhanced by the resonant excitation, and show clear one-to-one correspondence between the photoexcited state and the satellite state. The present results indicate that the resonant behavior is strongly influenced by the spin state.

References

[1] T. Hatsui et al., Chem. Phys. Lett., **284** (1998) 320.
[2] T. Hatsui et al., J. Synchrotron Rad., **6** (1999) 376.
[3] Y. Takata et al., J. Electron Spectrosc. and Relat. Phenom. **101-103** (1999) 443.
[4] Y. Takata et al., Chem. Phys. Lett., **287** (1998) 35.
[5] Y. Takata et al., J. Electron Specrosc. and Relat. Phenom. **93** (1998) 109.
[6] J. van Elp et al., J. Am. Chem. Soc., **116** (1994) 1918.

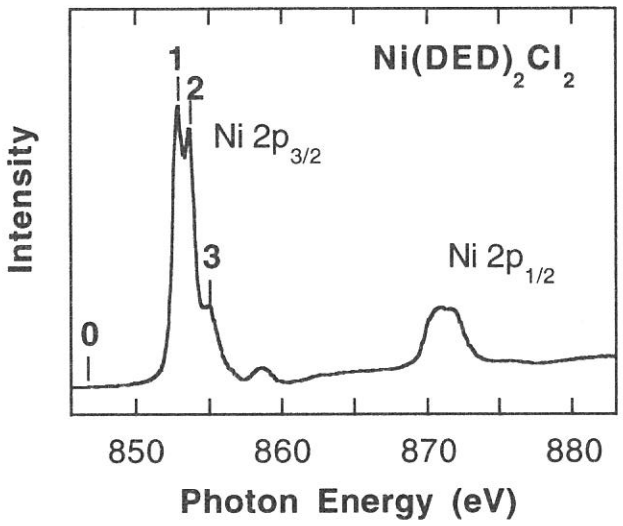

Fig. 1. Ni 2p photoabsorption spectrum of $Ni(DED)_2Cl_2$.

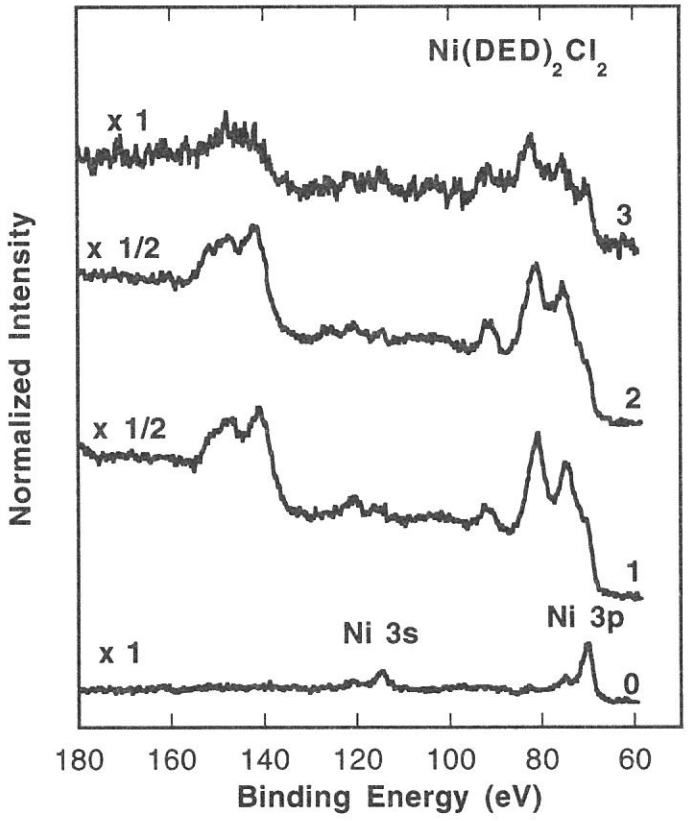

Fig. 2. Resonant photoelectron spectra in the Ni 3p and 3s regions of $Ni(DED)_2Cl_2$ at the photon energies marked in Fig. 1.

(BL2B1)

Removal of time-structure background in coincidence spectrum

Shin-ichi Nagaoka, Kazuhiko Mase,[A] Mitsuru Nagasono[B] and Shin-ichiro Tanaka[C]

Institute for Molecular Science, Okazaki 444-8585, [A]Photon Factory, Institute of Materials Structure Science, High Energy Accelerator Research Organization, 1-1 Oho, Tsukuba 305-0801, [B]MAX-lab, Beamline I511, Lund University, P.O. Box 118, 221 00 Lund, Sweden, [C]Department of Physics, Graduate School of Science, Nagoya University, Chikusa-ku, Nagoya 464-8602

In an energy-selected-photoelectron photoion coincidence (ESPEPICO) experiment, the pulses in the ion channel, triggered by a pulse in the energy-selected electron channel, are displayed as a function of the time delay between the two channels (i.e., the TOF). The TOF depends on the mass of the ions. By tuning to a peak of the photoelectron spectrum and measuring only the ions coincident with the electron emission, we can correlate an ionized-state with observation of an ionic fragment.

However, one experimental difficulty in ESPEPICO, as well as in any coincidence experiment, is differentiating between true and accidental coincidences [1,2]. Using a synchrotron-radiation apparatus operated in partial-filling mode makes this problem even more severe because the periodic accidental coincidences originating from the time-structure of the synchrotron radiation are superimposed on the ordinary accidental coincidences that are nearly independent of the TOF.

Figure 1a shows an ESPEPICO spectrum measured for (trifluorosilyl)(trimethylsilyl)methane (FSMSM) condensed on a Si(111) surface. The periodic structure is essentially the spectrum of the accidental coincidences, which show the modulation due to the time structure of the synchrotron radiation. Eberhardt et al. removed such a time-structure background by subtracting from the measured spectrum the shifted part of the spectrum containing only accidental coincidences [1,2]. We removed the time-structure background by performing fast-Fourier-transformation (FFT) on the ESPEPICO spectrum (that is, subtracting the ±177-ns component from the transformed spectrum), then performing an inverse FFT [3]. Figure 1b shows the time-structure background that was extracted with our method, and Figure 1c shows the difference between the spectra in Figures 1a and b. This technique worked so well that we were able to discern even weak true coincidence features very well. For example, a weak true coincidence peak can be seen at around 1.9 μs in Figure 1c, although it is difficult to discern the peak in Figure 1a.

When an ion is produced coincidentally with an energy-selected electron, the integrated intensity of a peak in the ESPEPICO spectrum (I) corresponds to the accumulated ion count. To estimate integrated intensity I, the time-structure background intensity (B) and the ordinary accidental-coincidence intensity (Z) should be subtracted from the total coincidence intensity (A). The error (r) for I inherent in the procedure described in the preceding paragraph was evaluated

as follows. I is given by

$$I = \sum_t \{A(t) - B(t) - Z(t)\}, \quad (1)$$

where t, $A(t)$, $B(t)$ and $Z(t)$ denote TOF, A measured at t, B at t and Z at t, respectively, and $A(t)>0$ and $Z(t)>0$. This summation is carried out over the TOF region of the corresponding peak. In the TOF region, $A(t)>B(t)+Z(t)>0$. Figures 1a and b show plots of $A(t)$ and $B(t)$ versus t, respectively. Assuming that the coincidence count obeys the Poisson distribution, error r is given by

$$r = \sqrt{\sum_t [A(t) + \{B(t) + Z(t)\}]}. \quad (2)$$

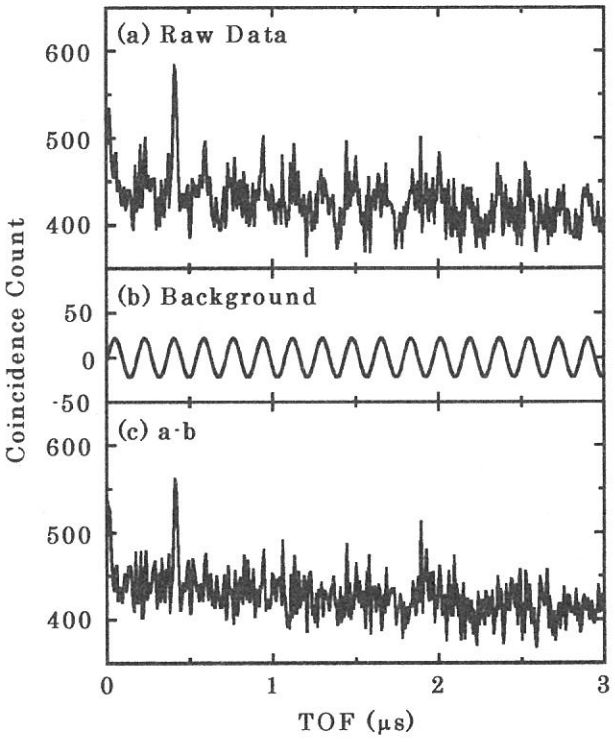

Let the total coincidence intensity at t in Figure 1c be $C(t)$. Because Figure 1c shows the difference between the spectra in Figures 1a and b, $C(t)$ can be written as

$$C(t) = A(t) - B(t), \quad (3)$$

where $C(t)>0$ in the corresponding TOF region. Equations (1) and (2) can thus be rewritten as

$$I = \sum_t \{C(t) - Z(t)\} \quad (4)$$

and

$$r = \sqrt{\sum_t \{C(t) + Z(t) + 2B(t)\}}. \quad (5)$$

In Figure 1, $r - \sqrt{\sum_t \{C(t) + Z(t)\}}$ was calculated to be 1.3 % of r for the peak at around 0.4 μs, but it was negligible for the peak at around 1.9 μs.

[1] W. Eberhardt, E. W. Plummer, I.-W. Lyo, R. Reininger, R. Carr, W. K. Ford, D. Sondericker, Aust. J. Phys. 39, 633 (1986).

[2] W. Eberhardt, E. W. Plummer, C. T. Chen, R. Carr, W. K. Ford, Nucl. Instrum. Methods Phys. Res., Sect. A 246, 825 (1986).

[3] S. Nagaoka, K. Mase, M. Nagasono, S. Tanaka, T. Urisu, J. Ohshita and U. Nagashima, Chem. Phys. 249, 15 (1999).

Figure 1. (a) ESPEPICO spectrum measured for FSMSM condensed on a Si(111) surface. This spectrum was obtained in coincidence with the electron emissions at a photon energy of 206 eV. Data collection time was 1200 s. The accidental coincidence reflects the time structure of the synchrotron radiation that was operated in a partial-filling mode with a period of 177 ns. (b) Time-structure background with a period of 177 ns. This time-structure background was extracted by using FFT. (c) Difference between spectra in Figures 1a and b.

(BL2B1)

Occurrence of different chemical shifts in Si:2*p* ionized state of $X_3Si(CH_2)_nSi(CH_3)_3$ (X=F or Cl, *n*=0-2) condensed on a Si(111) surface

Shin-ichi Nagaoka, Kazuhiko Mase,[A] Mitsuru Nagasono,[B] Shin-ichiro Tanaka,[C] Tsuneo Urisu, Joji Ohshita[D] and Umpei Nagashima[E]

Institute for Molecular Science, Okazaki 444-8585, [A]Photon Factory, Institute of Materials Structure Science, High Energy Accelerator Research Organization, 1-1 Oho, Tsukuba 305-0801, [B]MAX-lab, Beamline I511, Lund University, P.O. Box 118, 221 00 Lund, Sweden, [C]Department of Physics, Graduate School of Science, Nagoya University, Chikusa-ku, Nagoya 464-8602, [D]Department of Applied Chemistry, Faculty of Engineering, Hiroshima University, Higashi-Hiroshima 739-8527, and [E]National Institute of Advanced Interdisciplinary Research, Agency of Industrial Science and Technology, Ministry of International Trade and Industry, 1-1-4 Higashi, Tsukuba 305-8562

Synchrotron radiation has provided a powerful means to obtain information about core-level excitations, and the dynamic processes following the core-level excitations in molecules have long been a subject of interest. In contrast to valence electrons that are often delocalized over the entire molecule, the core electrons are localized near the atom of origin. Although core electrons do not participate in the chemical bonding, the energy of an atomic core-level in the molecule depends on the chemical environment around the atom. A shift in the energy levels of core electrons that is due to a specific chemical environment is called a chemical shift.

To elucidate the occurrence of different chemical shifts, we have studied the photoelectron spectroscopy and the *ab initio* calculation in the Si:2*p* core-ionized state of $X_3Si(CH_2)_nSi(CH_3)_3$ (X=F or Cl, *n*=0-2) [1-3]. The chemical environments of a Si atom bonded to three halogen atoms (Si[X]) and of Si bonded to three methyl groups (Si[Me]) are different from each other, so it seems likely that $X_3Si(CH_2)_nSi(CH_3)_3$ will show occurrence of different chemical shifts.

Figure 1 shows the photoelectron spectrum of $X_3Si(CH_2)_nSi(CH_3)_3$ condensed on a Si(111) surface. The high-resolution spectrum of the Si:2*p* peak is shown in the inset. The photoelectron spectra of the $F_3SiCH_2Si(CH_3)_3$ (FSMSM) and $F_3SiCH_2CH_2Si(CH_3)_3$ (FSMSE) have two peaks in the region of Si:2*p* electron emission (Figs. 1b and c). The peaks at the lower- and higher-energy sides are respectively assigned to Si[Me]:2*p* and Si[F]:2*p* electron emissions. In contrast, the peak due to the Si:2*p* electron emission of $Cl_3SiSi(CH_3)_3$ (MCDS) is not split (Fig. 1a), although the same energy-resolution of CMA was used for these three molecules. From these experimental results, we conclude that the occurrence of different chemical shifts at the two Si sites is clearly observed in molecules in which the two sites are located far apart. However, they are unlikely to be observed in molecules in which the two Si sites are closely located. To clarify the reason for the absence of these different chemical shifts in the latter molecules, we have made *ab initio* calculations.

Let the calculated energy gap between the Si[Me]:2p and Si[X, X=F or Cl]:2p core-eigenvalues be ΔE. In Fig. 2, the ΔEs of MFDS (X=F and n=0), MCDS (X=Cl and n=0), FSMSM (X=F and n=1), FSMSE (X=F and n=2) and FSMSP (X=F and n=3) are plotted as a function of the number of CH_2 groups between the two Si sites (n). For reference, the calculated energy difference between the Si:2p core-eigenvalues of SiF_4 ($SiCl_4$, CH_3SiF_3 and CH_3SiCl_3) and $Si(CH_3)_4$ is also plotted (assuming that n is ∞). Although ΔE is nearly constant or decreases slightly when going from FSMSP to FSMSE to FSMSM, it decreases rapidly when going from FSMSM to MFDS (MCDS). In MCDS, the small ΔE (Fig. 2) is thus consistent with the absence of different chemical shifts (Figs. 1a). The qualitative features of the present computational results are fully consistent with the experimental ones, so interpretation of the observed features of photoelectron spectra can be made on the basis of computational results [3].

[1] S. Nagaoka, K. Mase, M. Nagasono, S. Tanaka, T. Urisu and J. Ohshita, J. Chem. Phys. **107**, 10751 (1997).

[2] S. Nagaoka, K. Mase and I. Koyano, Trends Chem. Phys. **6**, 1 (1997).

[3] S. Nagaoka, K. Mase, M. Nagasono, S. Tanaka, T. Urisu, J. Ohshita and U. Nagashima, Chem. Phys. **249**, 15 (1999).

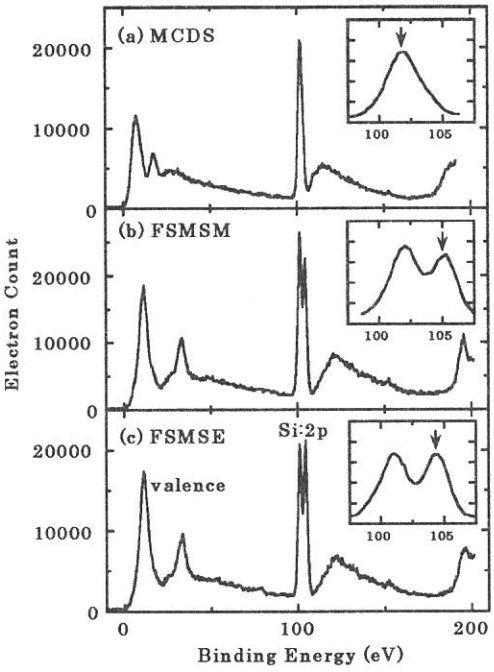

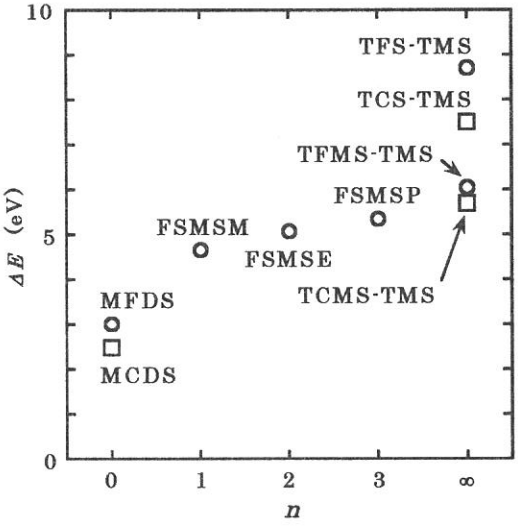

Figure 1 (left-hand side). Photoelectron spectra of (a) MCDS, (b) FSMSM and (c) FSMSE condensed on a Si(111) surface. The spectra a, b and c were taken at photon energies of 196.2, 206.6 and 206.6 eV, respectively. The horizontal scale of the spectra in the region of Si:2p electron emission is enlarged and shown in the insets. Each of the channels in the main spectra was measured for 0.2 s at a step of 0.5 eV, and each of those in the insets was measured for 0.5 s at 0.2 eV. In the measurement shown in the insets, an electric field across the ionization region was applied during the measurement.

Figure 2 (right-hand side). Plot of ΔE versus n in MFDS, MCDS, FSMSM, FSMSE and FSMSP.

(BL2B1)

Layer-resolved photoemission study of $CF_3CD(OH)CH_3$ on a Si(100) surface

Shin-ichi Nagaoka, Arinobu Nakamura,[A] Kazuhiko Mase[B] and Shin-ichiro Tanaka[C]

Institute for Molecular Science, Okazaki 444-8585

[A]Department of Chemistry, Faculty of Science, Ehime University, Matsuyama 790-8577

[B]Photon Factory, Institute of Materials Structure Science, High Energy Accelerator Research Organization, 1-1 Oho, Tsukuba 305-0801

[C]Department of Physics, Graduate School of Science, Nagoya University, Chikusa-ku, Nagoya 464-8602

The study of adsorbate properties and behaviors on substrates has attracted considerable attention. Chiang et al. previously reported the observation of layer-resolved shifts of photoemission spectra from physisorbed rare-gas multilayers [1]. The shifts were explained in terms of difference in final-state hole-screening energy. However, such a shift has not yet been found for molecules adsorbed on surface. In the present study, we have studied the photoemission spectra of $CF_3CD(OH)CH_3$ (TFIP-d_1) on Si(100) and have found that similar shifts can be revealed in the binding energies of the C:1s core-level, the O:1s core-level and the valence level. TFIP-d_1 is expected to be adsorbed on Si(100) like $CF_3CD(O(H)Si\{substrate\})CH_3$ [2], which is consistent with the results of NEXAFS.

TFIP-d_1 was prepared with the reaction of CF_3COCH_3 and $LiAlD_4$. The amount-regions of gas exposure corresponding to the monolayer coverage and the multiplayer coverage were determined by observing the development of the ion intensity as a function of the amount of gas exposure; the plot of the ion intensity versus the amount of gas exposure was discontinuous between the two regions. The experiments were performed using a double-pass cylindrical-mirror electron-energy analyzer (ULVAC-PHI) and a home-built time-of-flight ion-detection assembly coupled to a grasshopper monochromator (Mark XV) installed on the BL2B1 beamline [3].

Figure 1a shows the C:1s core-level photoemission spectrum of TFIP-d_1 monolayer on a Si(100) surface. The spectrum has three peaks whose assignments are given in the figure. The occurrence of different chemical shifts at the three C sites can clearly be revealed. The site-specific fragmentation of this molecule is very interesting [4].

Figure 1b shows the C:1s core-level photoemission spectrum of TFIP-d_1 condensed on a Si(100) surface (multilayer). The peaks in the spectrum of the multilayer are shifted by about 0.5 eV to higher binding energies from those of the monolayer. Similar shifts can also be found in the O:1s core-level and valence photoemission spectra (Figures 2 and 3); the amounts of the shifts are 0.7 and 1.4 eV, respectively. As in the case of rare-gas [1], the shifts might be explained in terms of difference in final-state hole-screening energy.

Further investigations are clearly needed on the reason of the spectral shift and the

site-specific fragmentation in this molecule.

[1] T.-C. Chiang, G. Kaindl and T. Mandel, Phys. Rev. B 33, 695 (1986).

[2] J. Yoshinobu, S. Tanaka and M. Nishijima, Appl. Phys. 60, 1196 (1991).

[3] S. Tanaka, N. Takahashi, K.-P. Lee and M. Kamada, J. Electron Spectrosc. Relat. Phenom. 80, 205 (1996).

[4] A. Nakamura, S. Nagaoka, K. Mase, S. Tanaka and T. Urisu, UVSOR Activity Report, 26, 100 (1998).

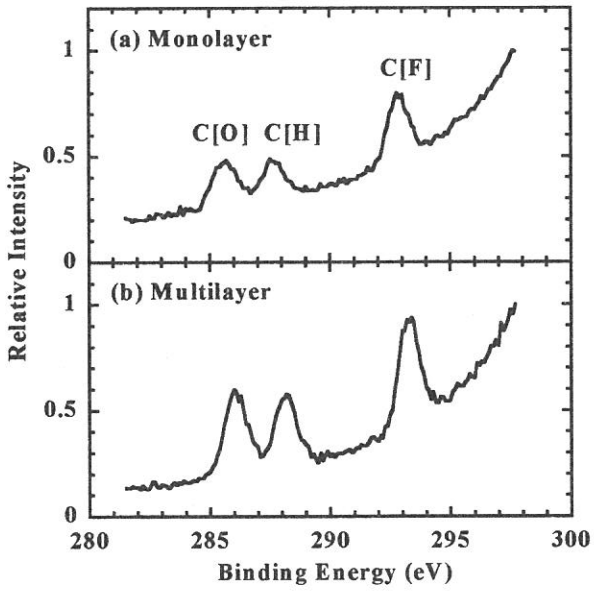

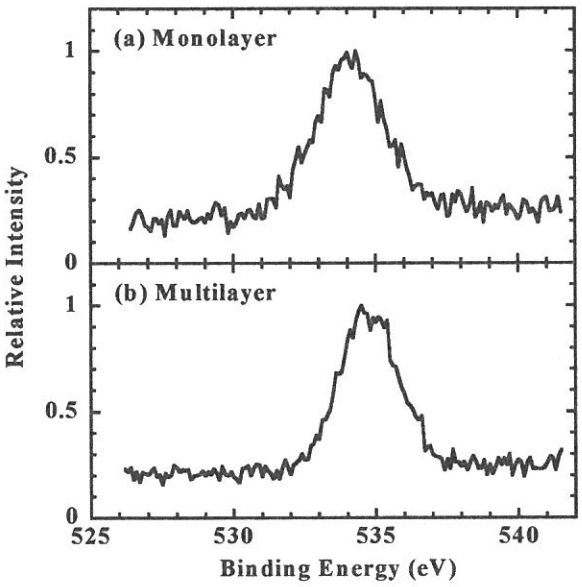

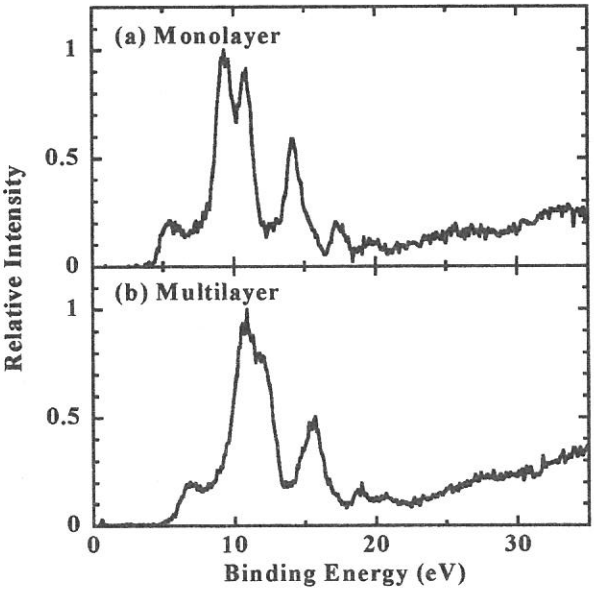

Figure 1 (upper left-hand side). C:1s core-level photoemission spectrum of TFIP-d_1 on a Si(100) surface. (a) Monolayer. (b) Multilayer. The assignments are given in the figure.

Figure 2 (upper right-hand side). O:1s core-level photoemission spectrum of TFIP-d_1 on a Si(100) surface. (a) Monolayer. (b) Multilayer.

Figure 3 (bottom). Valence-level photoemission spectrum of TFIP-d_1 on a Si(100) surface. (a) Monolayer. (b) Multilayer.

(BL5A)

Ultraviolet Photoelectron Spectra of $D0_3$-related $(Fe_{1-x}V_x)_3Al$ and $Fe_2VAl_{1-z}Si_z$ Alloys

Osamu YOSHIMOTO, Hideyoshi TANAKA, Shintaro YUASA, Masahiko KATO, Kazuo SODA, Masaaki KATO[A], Yoichi NINSHINO[A], Shin-ichiro TANAKA[B], and Masao KAMADA[B]

Graduate School of Engineering, Nagoya University, Furo-cho, Chikusa, Nagoya 464-8603

[A]*Nagoya Institute of Technology, Gokiso-cho, Showa, Nagoya 466-8555*

[B]*Institute for Molecular Science, Myodaiji, Okazaki 444-8585*

Recently, the $D0_3$-related pseudo-binary alloys $(Fe_xV_{1-x})_3Al$ have been received much attention because of their fascinating electronic and magnetic properties [1,2]. The alloy of the V composition $x = 0$, *i.e.* Fe_3Al is a well-ordered ferromagnetic metal of the $D0_3$ crystal structure with the Curie temperature T_C of 720 K. As the composition x is increased, T_C and magnetization of the pseudo-binary alloys are rapidly reduced, and their electrical resistivities exhibit a maximum at a temperature T_m near T_C and hence negative temperature dependence above T_m. Finally, the alloy with $x = 1/3$, *i.e.* the Heusler-type Fe_2VAl compound is in a marginally magnetic state, and its electrical resistivity shows semiconductorlike behavior suggesting an energy gap of about 0.1 eV and reaching 30 μΩm at 2 K. Low-temperature specific heat studies indicate a large enhancement of the effective electron mass and a substantial decrease in carrier concentration in Fe_2VAl. The Hall effect [3] and nuclear magnetic resonance [4] measurements also support the low carrier concentration. Several theoretical studies predict that Fe_2VAl is a nonmagnetic semimetal with a pronounced pseudogap of about 0.5 eV in its width across the Fermi level E_F [5-10]. The anomalous transport property is thought to arise from the spin fluctuation as well as the low carrier concentration rather than the existence of the band gap [1,2]. However, its ultraviolet photoelectron spectrum reveals a clear metallic Fermi edge with fairly large intensity [1,11]. Thus we have systematically investigated the valence-band photoelectron spectra of $(Fe_xV_{1-x})_3Al$ and $Fe_2VAl_{1-z}Si_z$. In $(Fe_xV_{1-x})_3Al$ with x larger than 1/3, its resistivity is higher than in Fe_2VAl, which may show a wider (pseudo)gap. In $Fe_2VAl_{1-z}Si_z$, E_F might be shifted by several hundreds meV in the rigid band model with a calculated density of states [10] at the Si composition $z = 0.2$. Here, we will report some preliminary results.

Photoelectron measurement was performed at BL-5A with a helical undulator [12], a spherical grating monochromator SGM-TRAIN [13] and a hemispherical analyzer (Omicron EA125HR) in an angle-integrated mode (the acceptance angle of 18°) under a pressure of 3×10^{-8} Pa. Specimens used in the present study were polycrystalline $(Fe_xV_{1-x})_3Al_{1-z}Si_z$ alloys prepared in the $D0_3$-related structure [1,2]. Specimens of 3 x 3 x 3 mm^3 in size were attached on a sample holder with conductive epoxy glue and cooled down to a temperature of about 80 K. Their surfaces were *in situ* cleaned with a diamond file for the photoelectron measurement. The total energy resolution was estimated to be 0.10 eV at the photon energy $h\nu$ of 40 eV and 0.12 eV at $h\nu = 75$ eV by measuring the Fermi edge of Au evaporated onto a plate of the sample holder. The origin of the binding energy *i.e.* E_F was also determined with the Au Fermi edge.

Figure 1 shows the valence-band photoelectron spectra of Fe_2VAl obtained at the first run after each cleaning procedure. The excitation photon energy $h\nu$ is indicated in the figure. The spectrum measured at $h\nu$

= 75 eV is similar to that reported so far [1]. However, a feature is noticed around the binding energy E_B of 6 eV in the spectrum obtained at $h\nu = 40$ eV. This feature seems to be attributed to the oxygen contamination due to the sample oxidation or condensation of molecules containing oxygen, and to become prominent at the low photon energy [14]. Unfortunately, we could not completely remove or prevent it in the present measurement.

The valence-band photoelectron spectra near E_F of Fe_2VAl, $(Fe_{0.62}V_{0.38})_3Al$ and $Fe_2VAl_{0.8}Si_{0.2}$ as well as Au are shown in Fig.2, where they are plotted so that the intensity may coincide with each other at $E_B \approx 0.15$ eV. As seen in the figure, no large gap can be recognized either in $(Fe_{0.62}V_{0.38})_3Al$ nor in $Fe_2VAl_{0.8}Si_{0.2}$, and the intensity at E_F is slightly low in Fe_2VAl compared with other compounds. For $Fe_2VAl_{0.8}Si_{0.2}$, these features seem consistent with a preliminary result on the temperature dependence of its resistivity, which shows a maximum at about 600 K. No indication of the gap and the relatively large intensity at E_F might show that the increase of the resistivity in $(Fe_xV_{1-x})_3Al$ with $x > 1/3$ arises from further spin fluctuation due to the lack of long range ordering. Rather sharp Fermi edge of Fe_2VAl, in comparison with Au, as well as its low intensity at E_F indicates a possibility of its low density of states above E_F [15]. Although the unoccupied states have not been investigated yet and the effect of the above-mentioned contamination is not clear, the present results suggest that the pseudogap in Fe_2VAl, if any, may be located higher in energy or its width may be smaller than expected.

References

[1] Y. Nishino *et al.*, Phys. Rev. Lett. **79**, 1909 (1997).
[2] M. Kato *et al.*, J. Phys.: Condens. Matter, *in press*.
[3] M. Kato *et al.*, J. Japan Inst. Metals **62**, 669 (1998).
[4] C.-S. Lue and Jr. J. H. Ross, Phys. Rev. B**58**, 9763 (1998).
[5] G.Y. Guo *et al.*, J. Phys.: Condens. Matter **10**, L119 (1998).
[6] D.J. Singh and I.I. Mazin, Phys. Rev. B**57**, 14352 (1998).
[7] R. Weht and W.E. Pickett, Phys. Rev. B**58**, 6855 (1998).
[8] M. Weinert and R.E. Watson, Phys. Rev. B**58**, 9732 (1998).
[9] A. Bansil *et al.*, Phys. Rev. B**60**, 13396 (1999).
[10] G. A. Botton *et al.*, Intermetallics, *in press*.
[11] K. Soda *et al.*, Jpn. J. Appl. Phys. Suppl. **38-1**, 496 (1999).
[12] S. Kimura *et al.*, J. Electron Spectrosc. Relat. Phenom., **80**, 437 (1996).
[13] M. Kamada *et al.*, Rev. Sci. Instrum. **66**, 1537 (1995).
[14] J.J. Yeh and I. Lindau, Atomic Data and Nuclear Data Tables **32**, 1 (1985).
[15] T. Sato *et al.*, Phys. Rev. Lett. **79**, 2254 (1999).

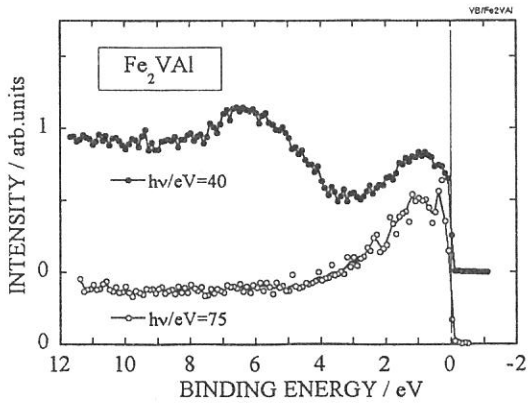

Fig.1 Valence-band photoelectron spectra of Fe_2VAl.

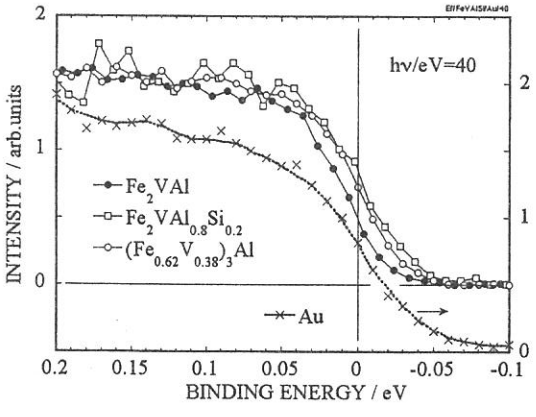

Fig. 2 Photoelectron spectra near the Fermi level.

(BL-5B)

Electronic Structures of Organic Salt DMTSA-BF_4 Using Photoelectron Spectromicroscopy

Yuichi HARUYAMA, Toyohiko KINOSHITA[A], Kazuo TAKIMIYA[B], Tetsuo OTSUBO[B], Chikako NAKANO[C] and Kyuya YAKUSHI[C]

Labortory of Advanced Science and Technology for Industory, Himeji Institute of Technology, 3-1-2 Kouto, Kamigori, Ako 678-1205

[A]*Synchrotron Radiation Laboratory, Institute for Solid State Physics, University of Tokyo, Tokyo 106-8666*

[B]*Faculty of Engineering, Hiroshima University, 1-4-1, Kagamiyama, Higashi-Hiroshima, 739-8527*

[C]*Institute for Molecular Science, Myodaiji, Okazaki 444-8585*

The 1:1 charge-transfer organic salt DMTSA-BF_4, where DMTSA is 2,3-dimethyltetraseleno-anthracene, have attracted the interest of many researchers because of the high electrical conductivity and metallic physical properties [1]. The electrical resistivity of DMTSA-BF_4 decreases from the room temperature to ~150K with a positive slope and DMTSA-BF_4 behaves as a metal. At about 150K the metal insulator transition is caused and the electrical resistivity below ~150K turn to increase with a negative slope as an insulator. It has been considered that the 1:1 charge-transfer salt becomes a Mott insulator due to the Coulomb interaction since the 1:1 charge-transfer salt has half-filled band. The origin of the metallic physical properties is not clear at present. In order to obtain the information on the electronic structures such as the band structure, density of states, and the orbital characters, we have performed the photoemission experiments for the organic salts DMTSA-BF_4. Since the size of DMTSA-BF_4 is not large enough to carry out the ordinary photoemission experiments, we used the photoelectron spectromicroscopy instrument as reported in Ref. 2.

Photoemission experiments were carried out by using a conventional UHV system (FISONS, ESCALAB-220i-XL) at a base pressure of 2×10^{-8} Pa [2]. Total instrumental energy resolution was 0.3~0.6 eV full width at half maximum (FWHM), depending on the photon energy ($h\nu$) in the energy range of 30~100 eV. Needlelike shaped single crystals of DMTSA-BF_4 and DMTSA were synthesized by electrochemical reduction [1]. The typical sample size used here was less than $2\times0.2\times0.1\mu m^3$. These samples were characterized by x-ray diffraction, electrical resistivity, magnetic susceptibility and ESR measurements [1]. The clean surface was obtained by scraping the sample surface using an edge of a razor. The cleanliness was confirmed by x-ray photoemission spectroscopy for the absence of extra features arising from the contaminations.

Figure 1(a) shows the photon energy dependence of the photoemission spectra for DMTSA-BF_4. From the photon energy dependence of the photoionization cross-section, the atomic orbital characters of the observed spectral features are determined. The features at ~1 eV, ~3 eV, and ~6 eV are predominantly derived from Se 4*p* states. The broad feature at ~8 eV is predominantly derived from C 2*p* and F 2*p* states. The features between 12 and 18 eV are predominantly from Se 4*s* and C 2*s* states. As shown in Fig. 1(b), the clear Fermi edge was not observed. It is suggested from the previous polarized reflection experiment [1] that DMTSA-BF_4 has a pseudo-one-dimensional band structure. No clear Fermi edge may be due to one dimensional electronic

structure for DMTSA-BF_4. In Figure 2, the Se 3*d* core-level photoemission spectrum for DMTSA-BF_4 is compared with that for DMTSA. The Se 3*d* core-level photoemission spectrum for DMTSA-BF_4 showed the tail at the higher binding energy side as compared with that for DMTSA. Although the difference of the Se 3*d* core-level photoemission spectra between DMTSA and DMTSA-BF_4 is not clear at present, there are some possibilities that the tail originates from the Doniach-Sunjic tail by the metallic nature and another component such as the different charge state and/or the surface component.

References

[1] J. Dong, K. Yakushi, K. Takimiya and T. Otsubo, J. Phys. Soc. Jpn. **67**(1998)971.

[2] T. Kinoshita, K. G. Nath, Y. Haruyama, M. Watanabe, S. Yagi, S. Kimura, and A. Fanelsa, J. Electron Spectrosc. Relat. Phenom. **92**(1998)165; T. Kinoshita, K. G. Nath, M. Watanabe, S. Yagi, S. Kimura, and A. Fanelsa, UVSOR Activity Report 1996, p.154.

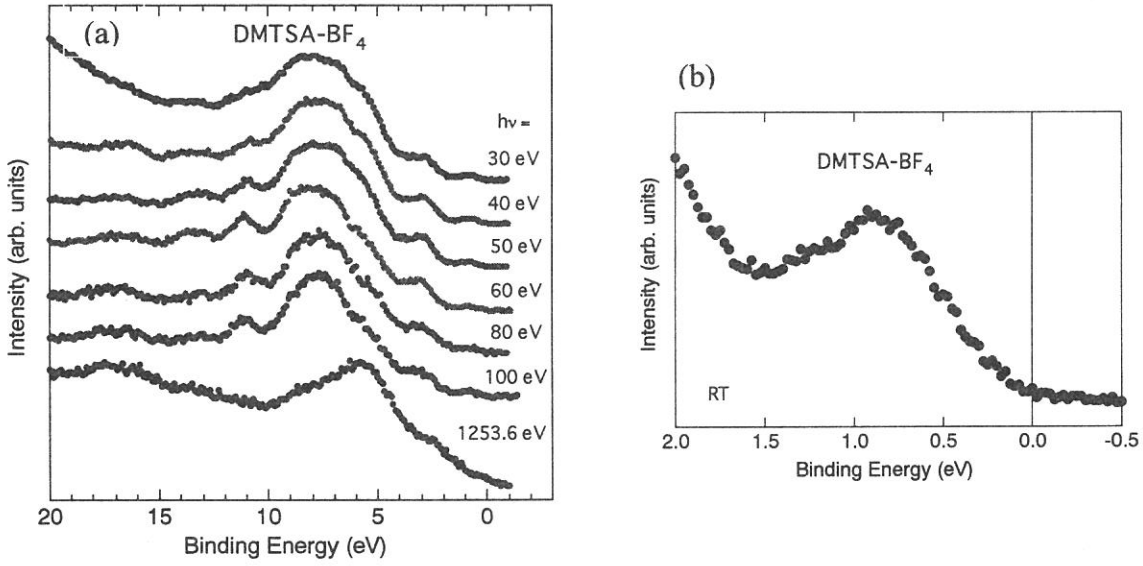

Figure 1 (a) The photon energy dependence of the photoemission spectra for DMTSA-BF_4. (b) The photoemission spectrum near the Fermi level. The detection area was ϕ50 μm.

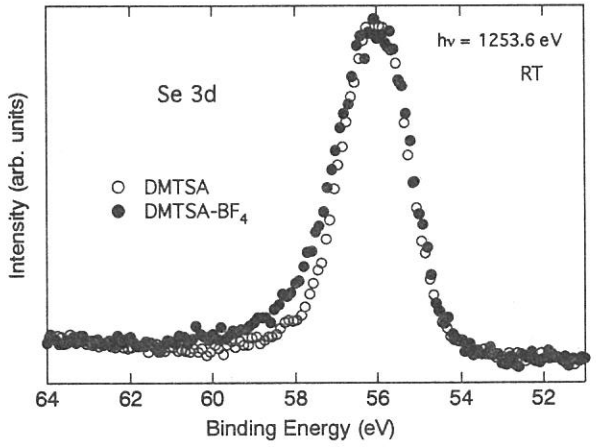

Figure 2 The Se 3*d* core-level photoemission spectra for DMTSA-BF_4(closed circles) and DMTSA(open circles). The detection area was ϕ50 μm.

(BL5B)

Photoelectron spectroscopic study on photo-induced phase transition in a spin crossover complex $Fe(2\text{-}pic)_3)Cl_2EtOH$

Masao Kamada, Yoichiro Doi,[A] Kazutoshi Fukui,[B] Yuichi Haruyama,[C] Syuji Asaka,[D] Takeshi Tayagaki,[E] Naoki Yonemura,[E] and Kouichiro Tanaka[E]

UVSOR Facility, Institute for Molecular Science, Okazaki 444-8585
[A] College of Engineering, Fukui University, Fukui 910-8507
[B] VUV-PhotoScience, Institute for Molecular Science, Okazaki 444-8585
[C] LASTI, Himeji University, Hyogo 678-1201
[D]Equipment Develop Center, Institute for Molecular Science, Okazaki 444-8585
[E]Faculty of Science, Kyoto University, Kyoto606-8502

In recent years, photon-induced phenomena attract much interest. For examples, photon excitation changes the crystal structures, magnetic and optical properties, and so on. These new phenomena are called as photo-induced phase transitions, which are expected to produce new properties of condensed matters.

In order to investigate the photo-induced phase transitions, optical spectroscopic techniques such as optical absorption and reflection have been mostly used, since these techniques can monitor the phenomena in a fast time domain. However, these techniques have some limitation. For examples, only narrow energy range in the valence electrons can be observed by the optical spectra. The purpose of the present study is to investigate the photo-induced effects on electronic states in wide energy range using photoelectron spectroscopy. We have been developing new techniques based on the combination of synchrotron radiation and laser in recent years. We will show the application of the technique to the present purpose.

Experiments have been carried out at a beam line BL5B, where a plane-grating monochromator provides photons in a wide energy range from 6 to 260 eV with a moderate resolving power and intense fluxes. A VG-microESCA system , which consists of XPS and UPS components with multi-channel detectors, was installed to this beamline during our beam time. A single crystal of $[Fe(2\text{-}pic)_3]\ Cl_2EtOH$ was grown at Kyoto university and was filed in a preparation chamber. The sample was attached on the holder of a flow-type He cryostat and was cooled down to about 40 K. The cw Ar^+ laser light was introduced in an analyzing chamber using an optical fiber to excite the sample during photoelectron measurements.

Figure 1 shows XPS spectra of Cl-2p states of $Fe(2\text{-}pic)_3]Cl_2EtOH$. Solid and broken lines represent the spectra observed at room temperature and 40K, respectively, while a dotted line shows the spectrum with laser excitation at 40K. It

is noted that the spectra are shifted to higher binding-energy side with cooling the sample, but no photo-induced effect is observed on Cl-2p state. Figure 2 shows N-1s spectra obtained under the same condition. It is obvious that the N-1s spectra are shifted to lower binding-energy side with cooling the sample and laser excitation causes the shift of N-1s to higher binding-energy side. The photo-induced spectrum at 40K is also in good agreement with the spectrum observed at RT. On the other hand, photoelectron spectra of Fe element, for examples Fe-3d spectra, are very complicate to explain (not shown here). The spectral structures were remarkably changed with temperature and laser excitation. The photo-induced spectrum at 40K is not agreement with that observed at RT.

It has been believed from the optical spectroscopic studies that $Fe(2\text{-pic})_3]$ Cl_2EtOH shows high-spin and low-spin states in Fe ions at RT and low temperatures, respectively, and that the low-spin state (low-temperature phase) is changed by photo-excitation to the high-spin state (high-temperature phase). However, the present experimental results indicate that the photo-induced phase transition of $Fe(2\text{-pic})_3]$ Cl_2EtOH is closely related to both Fe and N ions and is more complicate and interesting co-operative phenomenon.

Fig. 1. Photoelectron spectra of Cl-2p level in $Fe(2\text{-pic})_3]$ Cl_2EtOH. Solid and broken lines show the spectra at 40K and RT, respectively, while a dotted line represents the spectrum induced by laser excitation at 40K.

Fig. 2. Photoelectron spectra of N-1s level in $Fe(2\text{-pic})_3]$ Cl_2EtOH . Solid and broken lines show the spectra at 40K and RT, respectively, while a dotted line represents the spectrum induced by laser excitation at 40K.

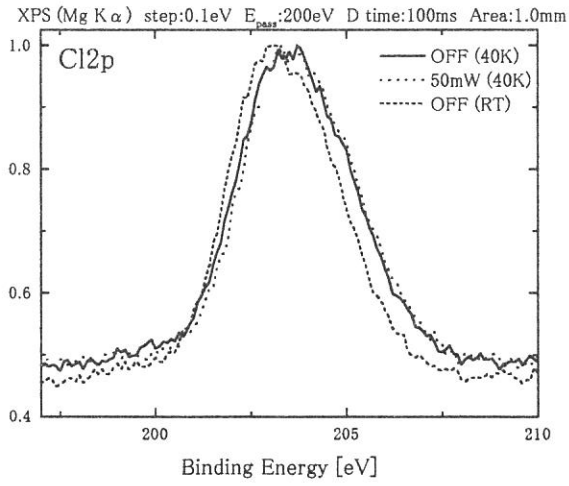

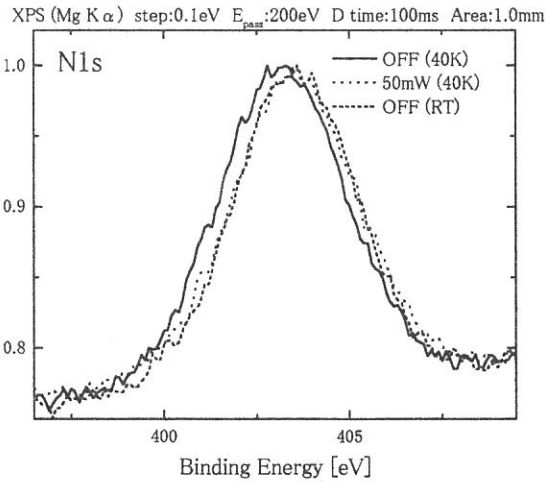

(BL-5B)

A Combined Study of Photoelectron Specrtomicroscopy and Laser Annealing For Si(111) Clean Surface

Yuichi HARUYAMA, Toyohiko KINOSHITA[A], Shin-ichiro TANAKA[B], Hideo MAKINO[C], Katsuo WADA[C], and Shinji MATSUI

Labortory of Advanced Science and Technology for Industory, Himeji Institute of Technology, 3-1-2 Kouto, Kamigori, Ako 678-1205

[A]*Synchrotron Radiation Laboratory, Institute for Solid State Physics, University of Tokyo, Tokyo 106-8666*

[B]*Faculty of Science, Nagoya University, Furo-cho, Chikusa-ku, Nagoya 464-8602*

[C]*Silicon Technology LTD, 897-20 Kyowa, Mochizuki, Kitasaku-gun, Nagano 384-2204*

The photoelectron spectromicroscopy is one of the attractive methods to investigate the electronic structure for various materials because a lot of applied usages are possible as compared with the ordinary photoelectron spectroscopy [1]. One of the advantages of the photoelectron spectromicroscopy is to measure the specific small area of the sample. Making the most of the advantage, we have performed the combined study of the photoelectron spectromicroscopy and the laser annealing. A merit of the laser annealing is that it is possible to anneal the specific small area of the sample by irradiating the focused laser light to the sample with less degassing and without the heating unit in the vacuum. In addition, the effect of the electric field used to keep the sample to high temperature is not needed if we use the laser annealing. Therefore, it is considered that the electronic structure at high temperature can be easily measured. As a typical example of the laser annealing, we report the electronic structure at high temperature for the Si (111) surface.

Figure 1(a) shows the experimental setup. Photoelectron spectromicroscopy experiments were carried out by using a conventional UHV system (FISONS, ESCALAB-220i-XL) at a base pressure of 2×10^{-8} Pa [1]. Total instrumental energy resolution at room temperature was 0.1~1.0 eV full width at half maximum, depending on the photon energy ($h\nu$) in the energy range of 21.2~1486.6 eV. The clean surface was obtained by annealing the sample at ~1200°C using the laser light irradiation ($h\nu$ = 1.165 eV) and checked by x-ray photoemission spectroscopy and LEED as shown in Figure 1(b). The temperature of the sample was measured with an optical pyrometer.

Figure 2(a) shows the temperature dependence of the photoemission spectra for n-Si (111) surface (P-dope, 9-14Ω) from room temperature to ~1200°C. At room temperature, three surface states were observed at ~0.2, ~0.8 and ~1.8 eV. With increasing the annealing temperature, the surface state at ~0.8 eV disappears. The temperature dependence of the spectral features obtained in our measurements is essentially identical to that previously obtained by Yokotsuka et al. [2]. However, we found that the shift of the photoemission spectra was observed at ~0.2 eV higher binding energy side under 0.04~0.89 W laser irradiation. With increasing the annealing temperature, the shift disappears at the laser power of 2.00 W. The shift at ~0.2 eV higher binding energy side was also observed at the Si 2p core level photoemission spectra as shown in Figure 2(b). It is considered that the observed rigid shift is caused by the surface photovoltage effect [3] induced by the laser irradiation.

Although we introduced the electronic structure at high temperature for the Si(111) surface, a lot of materials and surface systems cause the phase transition at high temperature. The combined study of the photoelectron spectromicroscopy and the laser annealing would become an effective method to investigate the electronic structure at high temperature.

References

[1] T. Kinoshita, K. G. Nath, Y. Haruyama, M. Watanabe, S. Yagi, S. Kimura, and A. Fanelsa, J. Electron Spectrosc. Relat. Phenom. **92**(1998)165; T. Kinoshita, K. G. Nath, M. Watanabe, S. Yagi, S. Kimura, and A. Fanelsa, UVSOR Activity Report 1996, p.154.

[2] T. Yokotsuka, S. Kono, S. Suzuki and T. Sagawa, Solid State Commun. **39**(1991) 1001.

[3] J. E. Demuth, W. J. Thompson, N. J. DiNardo and R. Imbihl, Phys. Rev. Lett. **56** (1986) 1408.

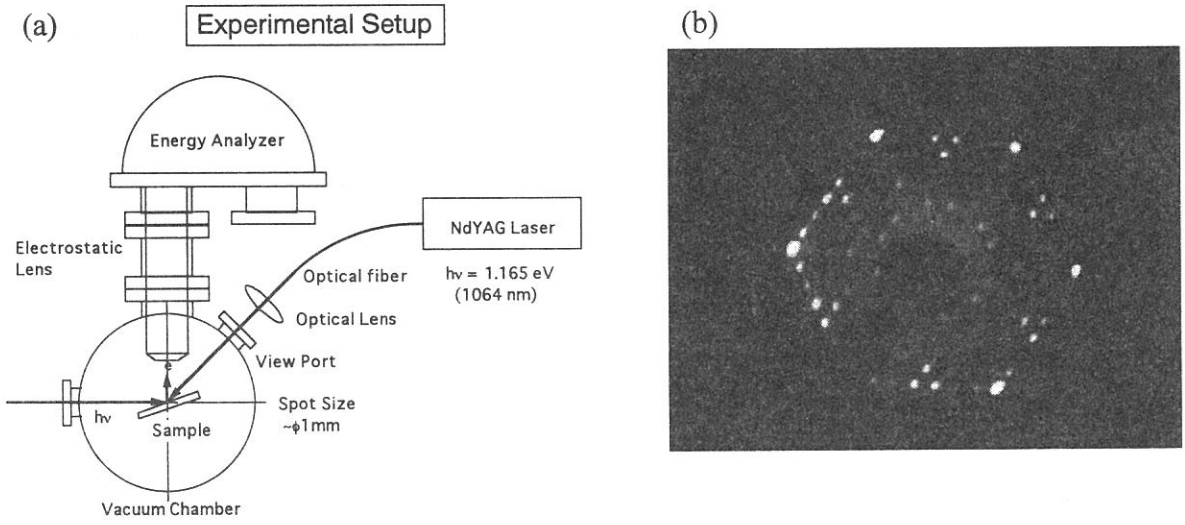

Figure 1(a) Schematic experimental setup. (b) A LEED pattern observed at ~54 eV electron energy after ~1200°C laser annealing.

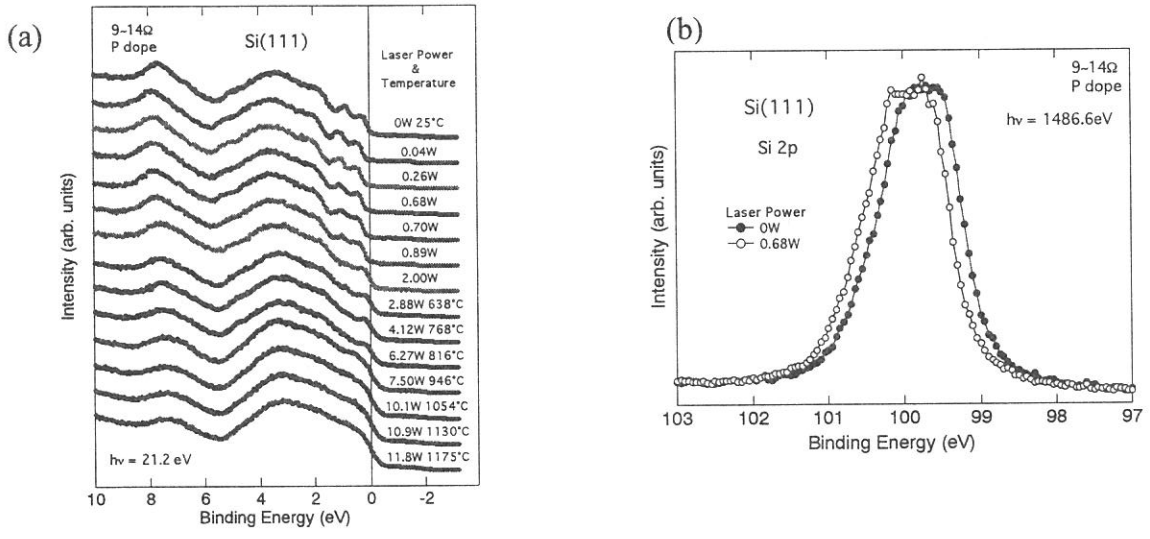

Figure 2(a) The temperature dependence of the photoelectron spectra in the valence band region for n-Si (111) surface. (b) Si 2p core level photoelectron spectra of n-Si (111) with and without laser irradiation.

(BL6A2)

Angle-resolved Photoelectron Spectroscopy of Si(111)-2√7x3-(Pb,Sn) Surface

J. Yuhara, K. Soda [1], S. Yuasa [1], O. Yoshimoto, K. Morita, M. Kamada [2]

Dept. of Cryst. Mat. Sci., School of Eng., Nagoya Univ., Chikusa-ku, Nagoya, 464-8603

[1] *Dept. of Nucl. Engineering, School of Eng., Nagoya Univ., Chikusa-ku, Nagoya, 464-8603*

[2] *Institute for Molecular Science, Myodaiji, Okazaki 444-8584*

Recently, it has been shown by means of LEED, AES, and RBS techniques that binary metal adsorbates of Pb and Sn on the Si(111) surface form a Si(111) 2√7x3-(Pb,Sn) surface at both Pb and Sn coverages of 0.5ML (1ML for Si(111) face = 7.8×10^{14} atoms/cm^2). STM images of the 2√7x3-(Pb,Sn) surface showed that there exist constant bright lines along [101] direction at both empty and filled states. The 2√7x3-(Pb,Sn) surface intrinsically has domain boundary, as shown in Fig.1. In this paper, ARUPS of the 2√7x3-(Pb,Sn) surface has been performed to study the dispersion relationship of the bright lines, with use of "single" domain 2√7x3-(Pb,Sn) surface .

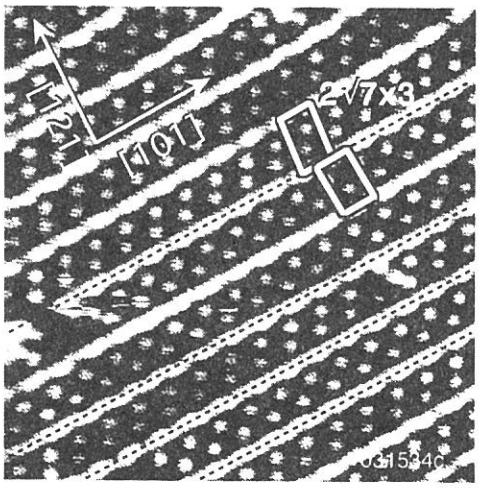

Fig.1 STM image of the Si(111)2√7x3-(Pb,Sn) surface at sample bias of -1.0eV. Dotted lines are domain boundary.

All the experiments were performed in the UHV chamber (8×10^{-10} Torr) at BL6A2. For ARUPS measurements, we used excitation photon energy of 26.1eV. The energy resolution and angular resolution at ARUPS measurements were 0.15eV and 1°, respectively. Specimens used were mirror-polished n-type Si(111) wafers with a miscut angle of ~2°. The "single" domain 2√7x3-(Pb,Sn) surface was prepared as followed. First, Sn of 0.8ML was deposited onto the Si(111)-7x7 surface at RT, and annealed at 550°C for 5min to form the 2√3x2√3+√3x√3-Sn surface at the Sn coverage of 0.5ML. Next, Pb of 0.8 ML deposited onto the 2√3x2√3+√3x√3-Sn surface was annealed at 300°C for 2 min.

A LEED pattern of the "single" domain 2√7x3-(Pb,Sn) surface is shown in Fig.2. The other domains are hardly seen. Surface Brillouin zones (SBZs) of the single domain 2√7x3 surface and 1x1 surface are shown in Fig.3. Symbols are 1x1 symmetry points. Typical spectra along the [101] direction are shown in Fig.4. The dispersion relationships along the [101] direction and [121] direction are shown in Fig.5 (a) and (b). Gray lines represent the projected bulk bands of the Si structures. Unique 2√7x3-(Pb,Sn) surface bands of S1 and S2 are clearly seen. The S1 band has peaks at Γ and K points, and the S2 band has peak at M point. The periodicity of S1 band does not match SBZs of both 2√7x3 and 1x1. Since there is no surface band across the Fermi level, the Si(111) 2√7x3-(Pb,Sn) surface is not metallic but semiconducting.

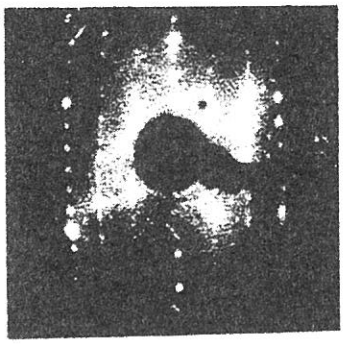

Fig.2 LEED pattern of a "single" domain Si(111)2√7x3-(Pb,Sn) surface.

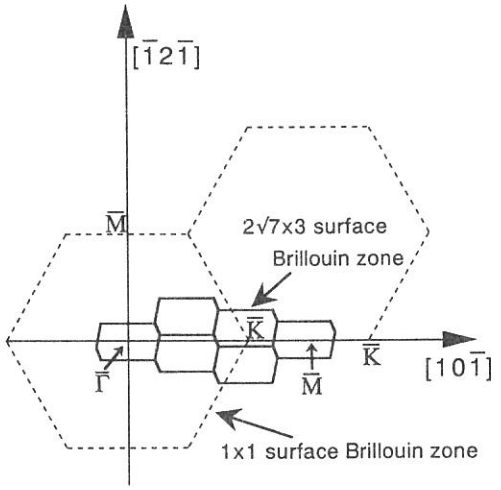

Fig.3 Surface Brillouin zones (SBZs) of the single domain Si(111)2√7x3-(Pb,Sn) surface and Si(111)1x1 surface.

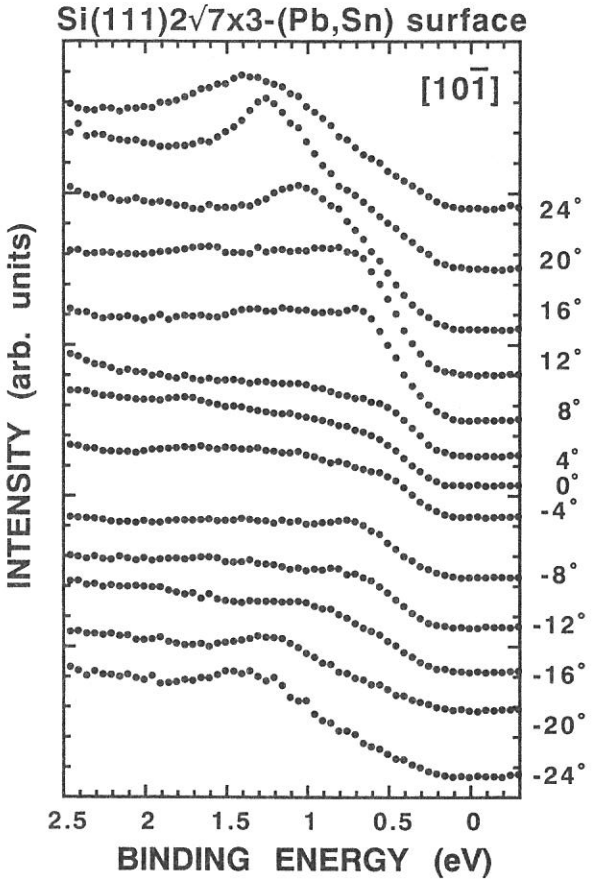

Fig.4 Typical ARUPS spectra for the "single" domain Si(111)2√7x3-(Pb,Sn) surface measured along the [101̄] direction.

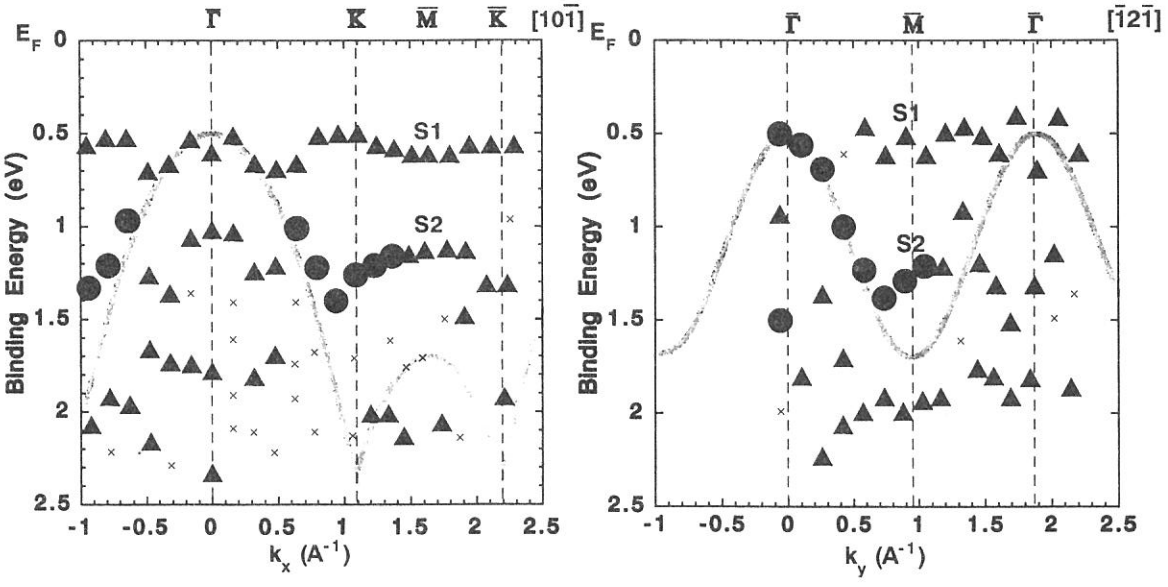

Fig.5 Band dispersion relationship along the [101̄] direction (a) and along the [1̄2̄1̄] direction (b).

(BL7A)

Structural analysis of molybdena/silica-alumina by means of Mo L_{III}-edge XANES

Hirofumi Aritani, Osamu Fukuda, Takashi Nishio, Hideyuki Yamane, and Seiichiro Imamura

Faculty of Engineering and Design, Kyoto Institute of Technology, Sakyo-ku, Kyoto 606-0962

Molybdenum-containing heterogeneous catalysts for olefin metathesis have been a great interest since Banks et al.[1] had reported the first observation. It is accepted fundamentally that reduced Mo ions such as Mo^{4+} and/or Mo^{5+} need to exist as the active center for metathesis. In the case of molybdenum-containing oxide catalysts, reductive pretreatment (with H_2 or CO) needs generally to reduce Mo^{6+} ions. However, we proposed previously that MoO_3/SiO_2-Al_2O_3 catalysts exhibit high activity for propene metathesis even at room temperature without reductive pretreatment.[2] In order to obtain the structural information details about the active molybdenum species for metathesis, the Mo L_{III}-edge XANES was applied to the supported molybdena systems. The XANES spectrum probes the orbitals of 4*d* character participating in the Mo-O bonds. The white lines of the spectrum are split, corresponding to the ligand field splitting of Mo 4*d* orbitals.[3]

Supported molybdenum catalyst samples were prepared by impregnation of each metal oxide support with an aqueous solution of ammonium heptamolybdate ($(NH_4)_6Mo_7O_{24}\cdot 4H_2O$) or acetone solution of bis(acetylacetonato)dioxomolybdenum ($MoO_2(acac)_2$). The oxide supports were SiO_2 (Aerosil), γ-Al_2O_3 (Nacalai, calcined at 873 K), and amorphous SiO_2-Al_2O_3 containing 28.6 wt% (JRC-SAH-1, indicated as SAH-1) and 13.8 wt% (JRC-SAL-2, indicated as SAL-2) Al_2O_3. The impregnating solution was stilled at room temperature and evaporated at 343 K for 6 h, and then, the paste was dried for overnight and calcined at 773 K for 6 h. The Mo *L*-edge XANES spectra were collected on a facility of BL-7A station of soft X-ray beam line at UVSOR, in the Institute for Molecular Science with 750 MeV of a ring energy. Each powdery sample was mounted on a carbon-tape, and then attached on a beryllium-copper dynode which was set to the first-stage of electron multiplier placed into a vacuum chamber. After the chamber had been evacuated ($< 3.0\cdot 10^{-7}$ Torr), the spectrum was recorded in a total electron yield (TEY) mode at room temperature, using the Ge(111) double-crystal monochromator ($2d$ = 0.6532 nm). The photon energy was calibrated by using Mo metal sample at Mo L_{III}-edge (2520 eV).

MoO_3/SiO_2-Al_2O_3 exhibit high activity for propene metathesis even at 293 K without reductive pretreatment, as described above. The metathesis reactivity (at 293 and 473 K) is summarized as (MoO_3/SAH-1 > MoO_3/SAL-2 > MoO_3/Al_2O_3 > MoO_3/SiO_2). Molybdena-rich MoO_3/SAH-1 (7.5 - 10.0 wt% as MoO_3) shows the highest catalytic activity. By the results of UV-Vis and ESR, it is concluded that molybdenum ions on SAH-1 can be easily reduced to form active species even by contact with propene, and thus, it shows a high activity without reductive pretreatment. The Mo L_{III}-edge XANES (TEY mode) of supported molybdena samples and reference compounds are shown in Fig. 1. The detailed interpretation of the spectra was described elsewhere.[4] In the case of MoO_3/SiO_2 and MoO_3/Al_2O_3 (prepared by means of AHM), tetrahedral Mo-O_4

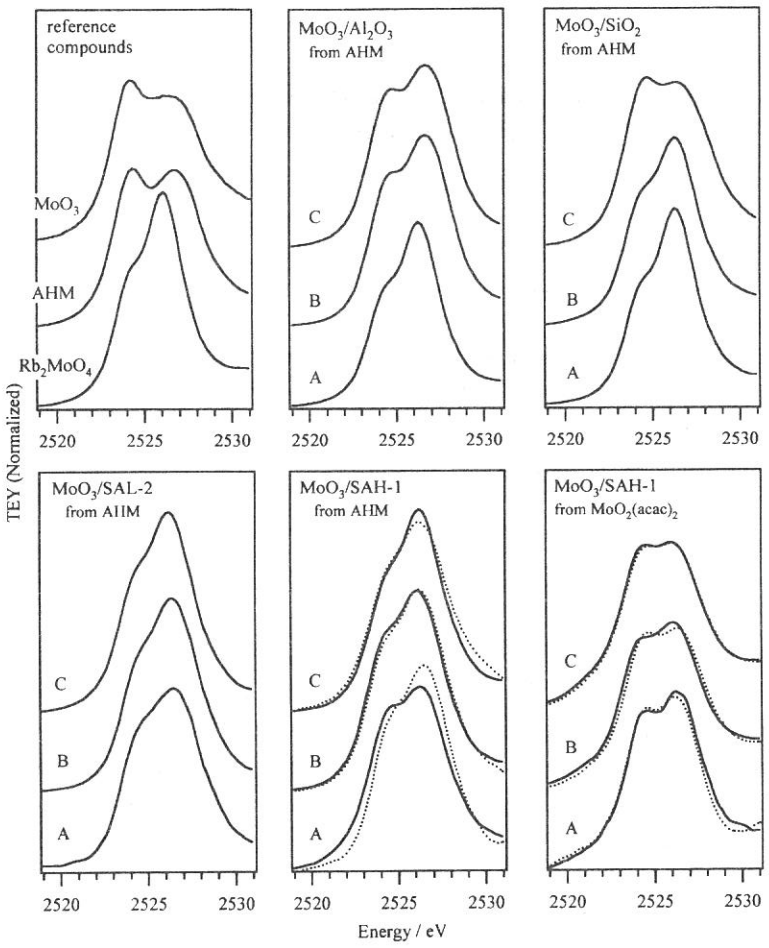

Fig. 1 Mo L_{III}-edge XANES of supported molybdena samples and reference compounds. Contents of MoO_3 are (A) 2.5, (B) 7.5, and (C) 15.0 wt%. Dotted lines are the spectra of each sample after the metathesis reaction at 293 K.

species are dominant at a low MoO_3 content (2.5 wt%). With an increase in MoO_3 content, polyanion-like Mo-O_6 octahedra coexist with tetrahedra. For 15.0 wt% MoO_3/SiO_2, the octahedral species exist mainly. These results support the conclusion reported previously by several workers.[5] On the other hand, the molybdena species supported on SiO_2-Al_2O_3 (SAH-1 and SAL-2) is almost occupied by the tetrahedron even at the higher MoO_3 contents. It is likely that the molybdena species in 2.5 wt% MoO_3/SiO_2-Al_2O_3 contains poly-anion-like octahedra partly, and it is almost absent after the catalytic reaction. For 7.5 and 15.0 wt% MoO_3/SAH-1, structural change of tetrahedral species is scarcely brought about by the reaction. It can be suggested that the formation of the bulk MoO_3 phase and/or large polyanion clusters proceeds hardly on SiO_2-Al_2O_3 because of peculiar support-interaction as reported.[6] In contrast, the polyanion-like octahedra coexist with tetrahedra on SAH-1 when $MoO_2(acac)_2$ is employed as the precursor. The structure of these species is little affected by the reaction. The study of the structural difference between these MoO_3/SAH-1 samples prepared from AHM and $MoO_2(acac)_2$ is now in progress.

We acknowledge Dr. E. Shigemasa and staffs of UVSOR for helpful assistance and support of the works in the BL-7A beamline.

1 R. L. Banks and G. C. Bailey, *Ind. Eng. Chem., Prod. Res. Develop.*, **3**, 170 (1964).

2 H. Aritani et al., *Chem. Lett.*, in press.

3 J. Evans et al., *J. Phys. Chem.*, **95**, 9673 (1991).

4 H. Aritani et al., *UVSOR Activity Report*, 1996, 208.; H. Aritani et al., *UVSOR Activity Report*, 1997, 210.; H. Aritani et al., *J. Phys. Chem.*, **100**, 19495 (1996).

5 H. Shimada et al., *J. Catal.*, **138**, 746 (1992).; H. Praliaud, In *Proc. 2nd International Conference on Chemistry and Uses of Molybdenum*, Climax Molybdenum Co., London, p. 195 (1976).

6 S. Rajagopal et al., *J. Catal.*, 147, 417 (1994).; S. Rajagopal et al., *J. Catal.*, 151, 192 (1995).

(BL7A)

Structural Analysis of Oxygen-coordinated Al(III) in Mullite by Means of X-ray Absorption Fine Structure

Hikoshiro ICHIHASHI, Shuji MATSUO, Tsutomu KURISAKI,
Takushi YOKOYAMA[1], and Hisanobu WAKITA*

Department of Chemistry, Faculty of Science, Fukuoka University,
Nanakuma, Jonan-ku, Fukuoka 814-0180, Japan
[1]*Department of Chemistry, Faculty of Science, Kyushu University,*
Hakozaki, Higashi-ku, Fukuoka 812-8581, Japan

*Corresponding author: wakita@SUNSP1.sc.fukuoka-u.ac.jp

Introduction

Light metal oxides are noticed as functional materials recently, and applied for ceramics and various catalyses. In particularly, aluminosilicate minerals as the light metal oxides are used well as materials of ceramics. However, the aluminosilicate minerals have not been made a fundamental study in detail, especially for a correlation between coordination and electronic structures around Al(III) or Si(IV), though there are aluminosilicate minerals with various oxygen-coordinated Al(III) in nature. We have investigated the electronic structures around Al(III) in the aluminosilicate minerals by an X-ray absorption fine structure (XAFS) method. A region of X-ray absorption near edge structure (XANES) on XAFS spectrum is useful to contain the structural information of the electronic state around an absorbing atom. In previous studies, we carried out the Al *K*-edge XAFS measurement for anorthite [$CaAl_2Si_2O_8$: four-coordinated to Al(III)], andalusite [Al_2SiO_5 : five- and six- (1 : 1) coordinated to Al(III)], and kaolinate [$Al_2Si_2O_5(OH)_4$: six-coordinated to Al(III)] in a series of aluminosilicate minerals, and obtained the relationship between the features of the XANES spectra for Al(III) in their aluminosilicate minerals and the coordination number around the Al(III). In this study, we investigate the structure around the Al(III) in mullite, one of a series of aluminosilicate minerals, by the XAFS method with being based on the result mentioned above. Strength of ceramics made of mullite depends on the structure and composition of mullite. However, the structure of mullite has been insufficiently studied, since mullite has a complicating structure. Therefore, it is worth study to reveal the structure of mullite.

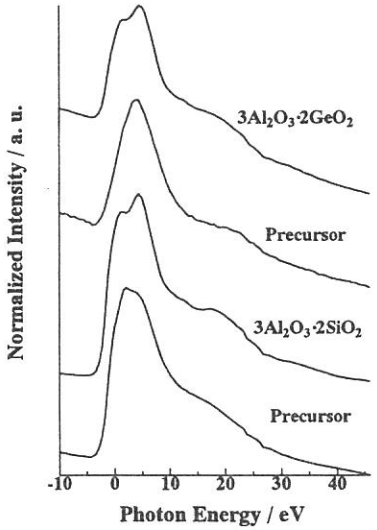

Fig. 1. Al K XANES spectra of noncrystalline mullites and noncrystalline mullite precursors.

Experimental

The Al *K* XAFS measurements were carried out at the BL7A of UVSOR in the Institute for Molecular Science. Two YB_{66} crystals as a monochromator are used combining with Si mirror. The storage ring was operated at 750 MeV. All of XANES spectra were measured by the total electron yield method. The samples in powder were mounted on CuBe photo dynode, and were attached to the photomultiplier tube. A series of mullites were prepared by adsorption of silicic acid on aluminium hydroxide. The detailed preparation method is described in a previous paper[1]. All samples (noncrystalline mullite precursors and noncrystalline mullites) are represented in terms of their composition as $3Al_2O_3 . 2(Si_xGe_{1-x}O_2)$.

Table 1. The enegy values of the Al *K* edge for $3Al_2O_3 \cdot 2(Si_xGe_{1-x}O_2)$ noncrystalline Mullites.

Composition	First peak(eV)	Second peak(eV)
Ge only	1.6271	4.4276
Si : Ge = 1 : 5	1.3179	4.7308
Si : Ge = 1 : 5	1.6271	3.8803
Si : Ge = 1 : 5	1.3043	4.7308
Si : Ge = 1 : 5	1.6271	3.8803
Si : Ge = 1 : 5	1.3179	4.7308
Si only	1.6271	4.4276

Results and discussion

Main peak positions on the Al *K* XANES spectra of a series of noncrystalline mullites and noncrystalline mullite precursors are presented in Fig. 1 and 2. In Fig. 1 and 2, the energy of abscissa axis was normalized with respect to the first peak top of aluminium metal as 0 eV. All of the XANES spectra of a series of model aluminosilicates present one maximum when aluminium is tetracoordinated, and two maxima when aluminium is hexacoordinated[2]. Their spectra of noncrystalline mullite precursors are not clearly observed two maxima, but their features are present an inflexion points in the spectra. Therefore, we conclude that all spectra contain two peaks, and the Al atoms of their noncrystalline mullites and noncrystalline mullite precursors are hexacoordinated.

Table 1 shows the peak top energy value of Al *K* edge for all samples. It was reported that slight variations in positions of the first maximum can be related to the Al-O bond character[3]. Their first maximum peak exists the slight variations, but the tendency of variations can not be explained satisfactorily. It is maybe due to the limit of the energy resolution of the beamline. Therefore, in our measurements, it is difficult to discuss the term of energy shift.

Fig. 3 shows the Fourier transformed EXAFS spectra of six samples. For gibbsite, the Fourier transformed EXAFS spectrum shows clearly the presence of the second neighbor atoms at about 3 Å. But all of the others do not show them clearly, and the comparison of thier first peaks didn't shift. It is maybe due to the limit of the energy resolution of the beamline. Because we consider that the Al-O distance of noncrystalline mullites and noncrystalline mullite precursors arise from compositional variation of silicon and germanium.

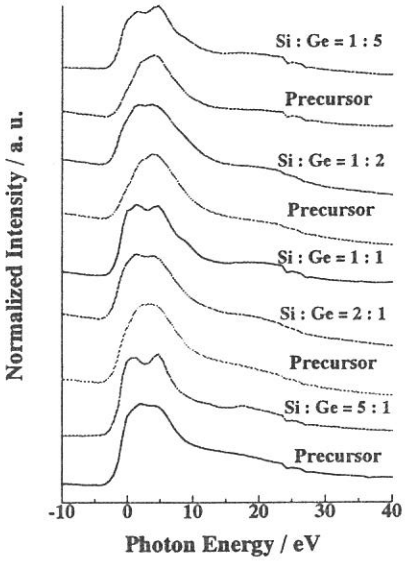

Fig. 2. Al *K* XANES spectra of noncrystalline mullites and noncrystalline mullite precursors. The compositions of them are represented as $3Al_2O_3 \cdot 2(Si_xGe_{1-x}O_2)$.

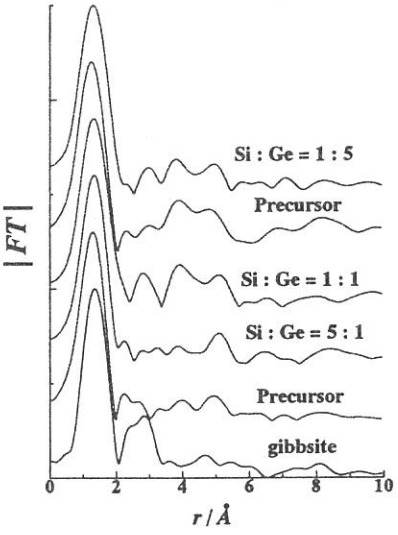

Fig. 3. The Fourier transforms of a series of noncrystalline mullites and noncrystalline mullite precursors. The com positions of them are represented as $3Al_2O_3 \cdot 2(Si_xGe_{1-x}O_2)$.

Conclusion

The Al *K* XANES spectra of a series of noncrystalline mullites and noncrystalline mullite precursors were measured. All Al atoms of them are hexacoordinated. The Fourier transformed EXAFS spectra of six samples derived, and the spectra didn't obtain a significant tendency. Further theoretical study is required.

References

1) Y. Ikeda, T. Yokoyama, S. Yamashita and H. Wakita, *Jpn. J. Appl. Phys.*, 32 (1993) 670-672.
2) J. Wong, Z. U. Rek, M. Rowen, T.Tanaka, F. Schäfers, B. Müller, G. N. George, I. J. Pickering, G. Via, B. DeVries, G. E. Brown Jr and M Fr ba, *Phys.*B 208&209 (1995) 220-222.
3) D. J. Jones, D. Grandjean and A. M. Flan *J. Non-crs. So.*, 147&148, (1992) 134-140.

(BL7A)

Analysis of Local Structure around Al(III) and Si(IV) in Mullite Containing Gerumanium(IV) by means of X-ray absorption fine structure

Hikoshiro ICHIHASHI, Shuji MATSUO, Kaori SHIROUZU, Tsutomu KURISAKI, Takushi YOKOYAMA[1], and Hisanobu WAKITA*

Department of Chemistry, Faculty of Science, Fukuoka University, Nanakuma, Jonan-ku, Fukuoka 814-0180, Japan
[1]*Department of Chemistry, Faculty of Science, Kyushu University, Hakozaki, Higashi-ku, Fukuoka 812-8581, Japan*

*Corresponding author: wakita@SUNSP1.sc.fukuoka-u.ac.jp

Introduction

Mullite is one of the aluminosilicates, and is excellent material for functional ceramics. The strength and crystallinity of the ceramics change by the ratio of Al (III) with Si (IV) and/or calcination temperature of mullite. As described in the UVSOR Activity report in 1998 and 1999, the Al *K* X-ray Absorption Near edge Structure (XANES) spectra of a series of model aluminosilicates, noncrystalline mullites and noncrystalline mullite precursors $\{3Al_2O_3 \cdot 2(Si_XGe_{1-X}O_2)\}$ were measured and analyzed in terms of Al-O distances and their bond characters. In particular, for noncrystalline mullites and noncrystalline mullite precursors $\{3Al_2O_3 \cdot 2(Si_XGe_{1-X}O_2)\}$, we conconcluded that the character changes of the mullites are particularly due to the change of Al-O bond character with the composition change of silicon and germanium. In this study, the Si *K* XANES spectra of a series of noncrystalline mullites and noncrystalline mullite precursors $\{3Al_2O_3 \cdot 2(Si_XGe_{1-X}O_2)\}$ were measured and discussed the electronic structures, especially, the properties of $3Al_2O_3 \cdot 2(Si_XGe_{1-X}O_2)$ mullites with the changes of Al-O, Si-O bond character were discussed.

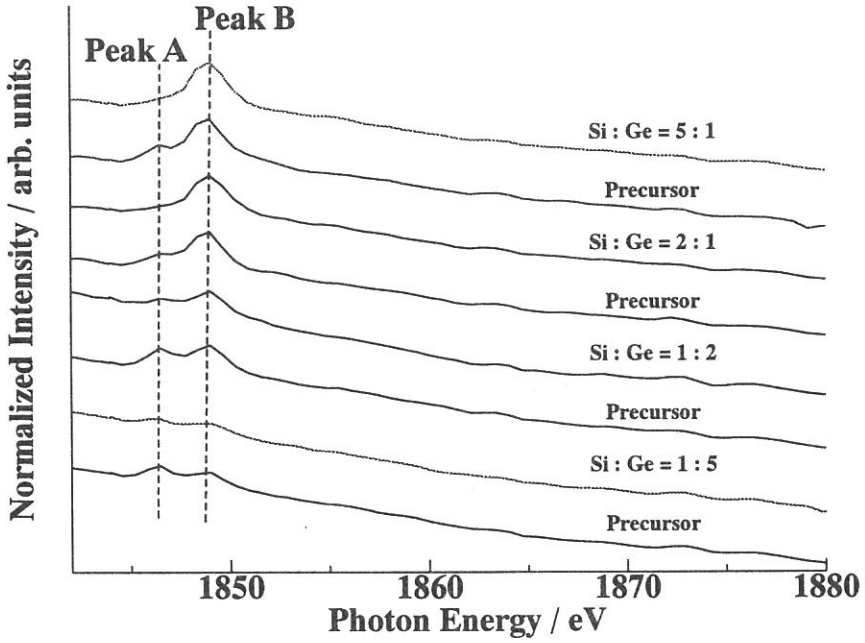

Fig. 1 Si *K* XANES spectra of a series of $3Al_2O_3 \cdot 2(Si_XGe_{1-X}O_2)$ noncrystalline mullites and noncrystalline mullite precursors.

Experimental

The Si *K* XANES spectra were measured at the BL7A in the UVSOR of the Institute for Molecular Science (Okazaki, Japan), a crystal monochromater beam line with Two YB_{66} crystals as a monochromator are used combining with Si mirror. The storage ring was operating at electron energy of 750 MeV. Powdered samples were dispersed on double-faced adhesive carbon tape mounted on copper slide and the signal detected as the total electron yield.

Results and discussion

Fig. 1 shows Si *K* XANES spectra of a series of $3Al_2O_3 \cdot 2(Si_XGe_{1-X}O_2)$ noncrystalline mullites and noncrystalline mullite precursors. It is immediately apparent that two peaks are present in the XANES spectra of all samples. As the results, the peak positions of the two peaks A and B on the Si *K* XANES spectra were nearly the same in the series. Therefore, from a simple fingerprint basis, the Si atoms seem to consist of the SiO_4 tetrahedral structure[1]. The presence of two peaks on the XANES spectra probably is due to two different Si-O distances. It was noted from previous report that the strength of peak B on Si *K* edge increases with increasing the Si composition of mullite. So, the first, it is due to the increase of Si component, that is the strength of observed spectra increases with increasing the composition of the absorbing atom Si. The second, it is reported that Peak B can be assigned the transition from Si 1s orbital to Si 3p-like orbital (3s/3p)[2], therefore, the feature of the Si *K* XANES spectra of mullite depends on a distribution of Si 3p-like orbital.

Conclusion

The Si *K* XANES spectra of a series of noncrystalline mullites and noncrystalline mullite precursors $\{3Al_2O_3 \cdot 2(Si_XGe_{1-X}O_2)\}$ were measured. These XANES spectra were used as a fingerprint study of the structure of the mullites and mullite precursors. All Si atoms of them are tetracoordinated. The feature of the Si *K* XANES spectra of the mullites probably depends on a distribution of Si 3p-like (Si 3s/3p) orbital. But it is not observed that the effect of Al-O bond character is due to the Si-O bond character change. Further theoretical study is required.

References

1) P. Colomban, D. J. Jones, D. Grandjean and A. M. Flank, *J. Non-Cryst. Sol.*, 147&148 (1992) 135.
2) D. Li, G. M. Bancroft, M. Kasrai, M. E. Fleet, X. H. Feng, K.H. Tan and B. X. Yang, *Sol. Sta. Com.*, 87(1993) 613.

(BL7A)

Thickness effects of photoluminescence from lithium bromide film excited with soft x-rays in Br-L edge energy.

Tokuo MTSUKAWA, Fumiaki MITANI and Toyohiko KINOSHITA*

Naruto University of Education, Naruto 772-8502

**Institute for Solid State Physics, The University of Tokyo, Tokyo 106-8666*

(5:Solid- & liquid-phase spectroscopy; soft x-ray, absorption, photo-luminescence)

We have measured sample thickness dependence of photoluminescence excitation spectra from vacuum evaporated LiBr film excited in the photon energy region of Br-L_3 absorption edge. Br-L spectra had become possible to measure by the use of YB_{66}[1] crystal as monochromator crystals at the BL7A beam line. We had obtained Br-L absorption spectra of alkali bromides by the transmission methods and photoluminescence yield spectra from thin samples excited in the energy region. In the case of fine powder samples, the excitation spectra show inverted profiles of absorption spectra in the case of LiBr fine powder sample, whereas other alkali bromides show same profile as the absorption spectra. It had been considered that it might be due to the difference of the effective sample thickness In order to observe the change with sample thickness, excitation spectra were measured on LiBr thin films prepared by vacuum evaporation with different thickness. Although the results show no existence of inverted feature, the intensity of excitation spectra are found to show characteristic variation with sample thickness.

Experiments were performed at the BL7A with YB66 monochromator crystal. Several modification were applied for the beamline. A sample preparation chamber were attached to the sample chamber to evaporate samples in separated place. Sample were prepared with vacuum evaporation on to a collodion film and transferred to the sample chamber for each measurements on every sample with different thickness. Evaporation were repeated over the one sample film after a measurement. The thickness of evaporated film was monitored by a quartz frequency monitor.

A photo-multiplier tube was installed at 45 degree to incident light direction through a quartz focusing lens of 20mm diameter at 200mm from the sample position. A electron-multiplier with Be-Cu anode was set behind the sample film, and absorption spectra were simultaneously obtained by a transmission method getting along with the excitation spectra.

Figure 1 shows a comparison of the excitation spectra with different film thickness . The thickness were given by the frequency shift of the quartz thickness monitor. No correction, nor estimation of the thickness was made because of lack of reference value of the density of dehydrate LiBr. In the figure the absorption spectrum is also shown with a dashed curve for a comparison. Spectral features are all common among the samples of the different thickness and with the absorption spectrum except the intensity distribution. As the thickness are small, it is apparent that the photoluminescence intensity increases rapidly.

Figure 2. shows a change of luminescence intensity measured at the energy below the absorption edge, the first absorption peak and second peak, which are shown by arrow A, B and C in figure 1, respectively. It is found that the change is presented quite well by a quadratic curve as shown in the figure by solid curves. That of C is given by a bold dashed curve, which has not minimum point whereas the other have minimum at around 2 kHz thickness. Intensity of the photoluminescence from thin film, excited with x-ray, increases as a function of quadratics of film thickness, not but linear function.

The luminescence intensity depends on the whole amount of creation of inner core holes, and the amount may depends on dose of absorbed x-ray, thus it may be considered to be proportional to the thickness of the sample. The intensity of the light may be unchanged since alkali halides are transparent in visible and uv region, thus no self-absorption effects are considered. We had obtained quantum efficiency spectra, ratio spectra of the luminescence and the dose spectra. The dose spectra are given by (I_0-I) spectra, where I_0 is incident x-ray spectra and I is transmitted x-ray spectra. They increase with sample thickness and appear to have maxmum structures at the same position as the excitation spectra. Figure 3 shows plots of the quantum efficiency at the point A,B and C against sample thickness. The figure show that quantum efficiency of A, B and C are not only linearly changes against the sample thickness as the samples are thin, but also they appear to converge to zero at thickness of about 2.5kHz commonly among A, B and C,. If it is true, it suggest that there is a threshold in the sample thickness to excite the photoluminescence by x-ray.

Fig.1

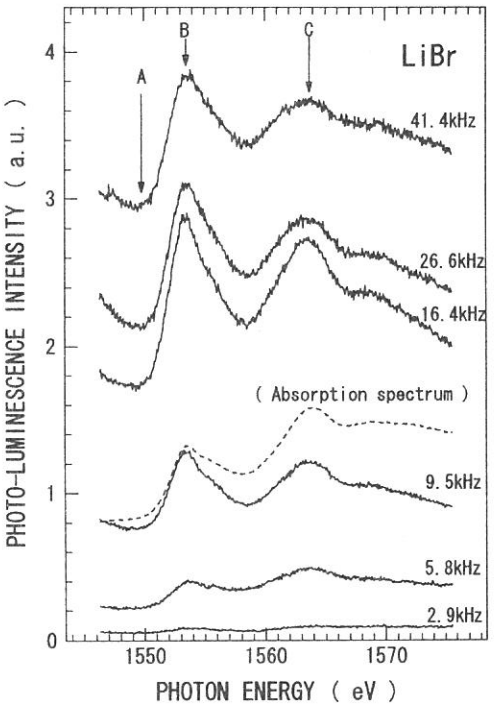

Fig.2

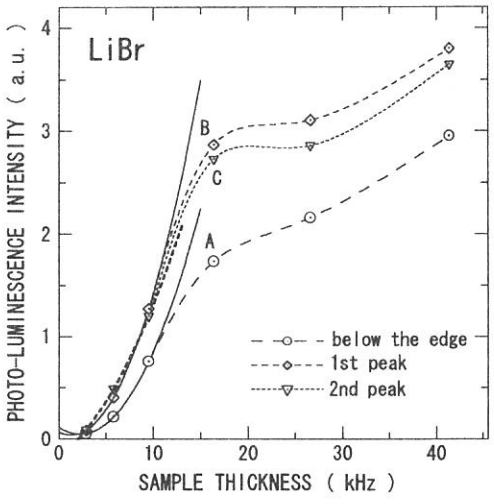

Fig.3

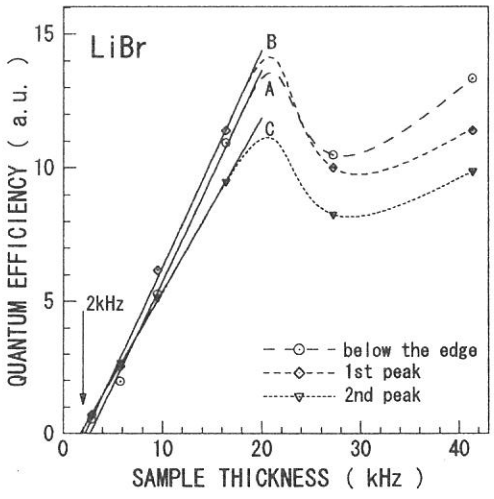

(BL7A)

Br-L_3 absorption spectra and excitation spectra of photoluminescence of alkali bromides.

Tokuo MATSUKAWA, Hiroaki OKUTANI and Toyohiko KINOSITA*)

Naruto University of Education, Naruto 772-8502

**Institute for Solid State Physics, The University of Tokyo, Tokyo 106-8666*

(5: Solid- & liquid-phase spectroscopy 2; soft x-ray, absorption , photo-luminescence)

Soft x-ray excitation spectra of luminescence were measured in Br-L_3 region as well as soft x-ray Br L_3 absorption spectra of alkali bromides. The photon energy of Br L edge exist at around 1500eV, where only few spectroscopic study is reported. One of the reason is that a proper monochromator crystal has been poor. At the BL7A beam line, stable spectroscopic works had become possible by the use of YB_{66} crystal in the region. The beam line was operated at the 4T-wiggler mode. The beam line is composed with a double crystal monochromator. By using wiggler, usable energy extends up to about 5 KeV and the intensity raises of the two order in the 1500eV region. The YB66 crystals used were commercial products synthesized by the Crystal Systems Inc.,Yamanashi, Japan. We had performed Br L absorption measurements on alkali bromides in order to check the availability. The experiments were performed on thin powder samples. The absorption spectra were obtained by the total photoelectron yield. The excitation spectra were obtained simultaneously with recording the intensity of the visible (ultraviolet) light from the sample.

Figures 1 to 4 show comparisons of the excitation spectrum and the absorption spectrum of four bromides, respectively. Thin curves show the absorption spectra and bold ones the excitation spectra. The absorption spectra have a series of fine structures at the edge commonly. The intensity distribution and the number are the similar to Cl-L spectra of alkali chlorides, though the Br spectra don't show sharp peak structures as Cl spectra. This is due to the restricted resolution at much more higher energy and the difference of the life time broadening of the core-level. The Br L spectra show no overlap structures because of the large separation of around 50eV between L_2 and L_3 levels. Thus the week and shallow structures in Br spectra may be explained as the exiton absorption peaks as chlorides.

The excitation spectra appear to follow the features of the absorption spectra, except that of LiBr. In the case of LiBr, the luminescence intensity drops at the threshold of the absorption edge. In the higher energy region luminescence yields shows some structures which corresponds absorption structures as peaks to dips. Thus the luminescence excitation spectrum of LiBr shows inverted profiles of the absorption spectrum. It is a well known phenomenon in the case the luminescence excitation spectra excited with x-ray. Emura et al. discussed the phenomena according to a phenomenological model. They showed that the excitation spectra changes the profiles among the effective thickness of samples. The results shows that the excitation spectra

change their spectral features as the effective thickness change, and finally reach the inverted profiles of absorption spectra. If it is true, our results of NaBr, KBr and RbBr are the case of the samples with enough thin effective thickness. Then, LiBr is a special case or might be due to a different condition of the sample preparation. Although we prepared the sample with fine powders as thin as possible, LiBr is deliquescence and fine powders crystallize to form a hydrate. Then effective thickness of the sample might be increase. Even though the sample in this case is that of a hydrate, the spectral features of the absorption spectrum presents the same features of non-hydrate which had been measured on a vacuum evaporated thin film using a dehydrate sample.

Fig.1

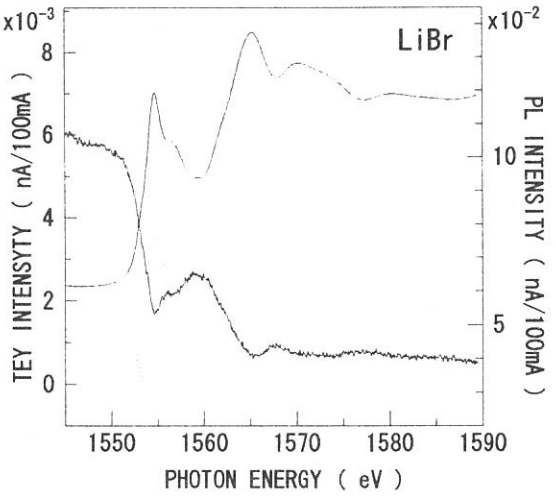

Fig.2

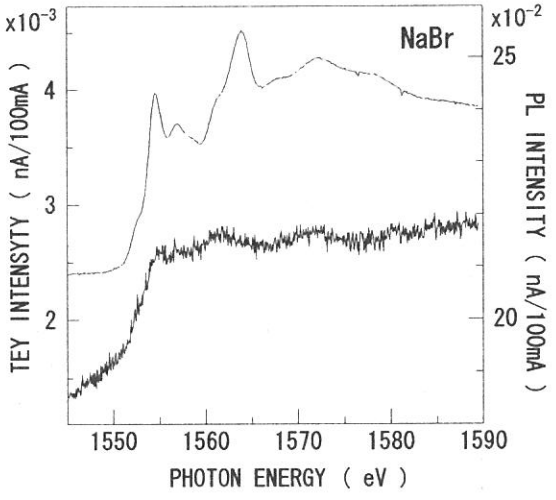

Fig.3

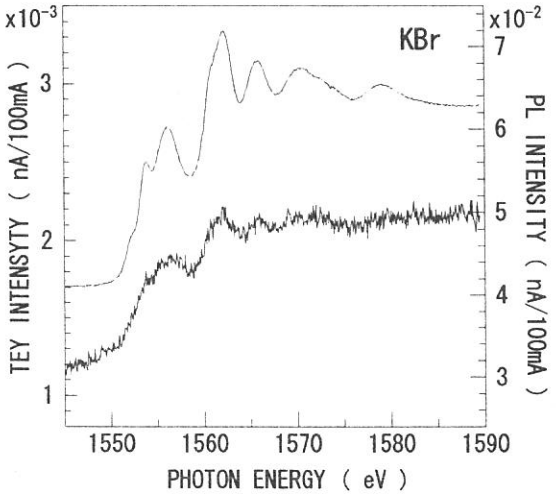

Fig.4

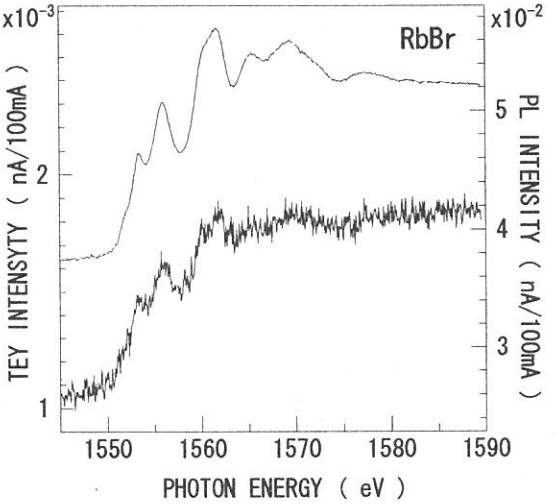

(BL7A)

Local structure around S in permanently densified GeS_2 glass

*Koichi MIYAUCHI, Masanori SHOJIYA, Yoji KAWAMOTO and Noriyuki KITAMURA**
Division of Molecular Science, Graduated School of Science and Technology, Kobe University, Nada, Kobe 657-8501, Japan
**Department of Optical Materials, Osaka National Research Institute, AIST, Midoriga-oka Ikeda 563-8577, Japan*

When glasses are treated under high pressures, significant increases in density are observed even after removal of the applied pressures. This permanent densification phenomenon of glass was demonstrated for the first time by Bridgman and Simon [1]. This permanent densification phenomenon is of importance from a practical point of view because it may be applied to control functions such as optical, electrical and mechanical properties without changing glass composition. The permanent densification phenomena have been investigated on various kinds of oxide and chalcogenide glasses [2,3]. On chalcogenide glasses, for example, the effects of high-pressures on various properties have been extensively investigated [3]. However, structural studies of permanently densified chalcogenide glasses are very few. On the structure of densified GeS_2 glass, for example, there is only one report, though the presumed structural changes are based on a change of the optical absorption-edges measured in situ under high-pressures [4].

GeS_2 glass was prepared from metallic Ge and elementary S according to the procedure described previously [5]. The prepared glass was annealed at the glass-transition temperature determined by a DTA analysis. Permanent densification of the GeS_2 glass was carried out with a 6-8 multi-anvil high-pressure apparatus under 1.5, 3.0, 4.5, 6.0 and 9.0 GPa at 270°C. The permanent densification was retained after the removal of the pressure and temperature. The densities and the absorption-edge energies in the visible region on permanently densified GeS_2 glasses are shown in Fig. 1. The density increased with pressure until 6.0 GPa and then reached to a constant value under further increased pressure. The absorption-edge energies in the visible region shifted toward low energies with pressure until 6.0 GPa and then reached a constant value under further increased pressure.

All the densified GeS_2 glasses have the same composition so that the changes of physicochemichal properties are attributable to structural changes by high-pressure treatments. Especially the shift of the absorption-edge energies is related to the molar volume and the Ge-S bond distance, as referred by Xu and Ching [6]. Therefore we investigated the local structure around S in undensified and densified GeS_2 glasses.

The XAFS measurements were carried out at BL-7A under ambient temperature using a Total Electron Yield method. A monochromater with two flat Ge(111) (d = 3.266) was used. The S-K XAFS absorption data were collected in the energy range from 400 eV on the low energy side of S-K absorption edge (2471 eV) to about 1200eV on high energy side. Analyses of EXAFS data were performed by using the program WinXas97. In the least square curve fitting procedure, the theoretical EXAFS parameters calculated from FEFF7 code [7] were used.

Fig. 2 shows the S-Ge atomic distance plotted against the applied pressure, together with the experimental error bar. The S-Ge atomic distance extended slightly with pressure untill 6.0 GPa and then reached a constant value under further increased pressure. The pressure dependence of S-Ge bond length corresponds to that of absorption-edge energy in the visible region. Thus, both are strongly related.

The XANES spectra of undensified and densified GeS_2 glasses and the α- and β-GeS_2 reference crystals were shown in Fig. 3. In the figure, solid lines indicate experimental spectra and dashed lines indicate combined spectra of α- and β-GeS_2 with given ratios. As the linkage manner of GeS_4 tetrahedra there are two kinds of manners; corner-sharing (linkage by one S) and edge-sharing (linkage by two S). The former exists in α- and β-GeS_2; while the latter is present only in α-GeS_2. A comparison of both spectra indicates that the S-K XANES spectra profile of GeS_2 glass varied from α-GeS_2 glass-like to β-GeS_2-like. Therefore it is concluded that the fraction of edge-sharing in the linkage of GeS_4 tetrahedra decreases with densification. This is also supported by a decrease of the peak due to Ge-Ge distance in edge-shared GeS_4 tetrahedra observed in X-ray differential radial distribution curves of undensified and densified GeS_2 glasses.

References

[1] P. W. Bridgman and I. Simon, J. Appl. Phys. 24 (1953) 405
[2] S. Sakka and J. D. Mackenzie, J. Non-Cryst. Solids 1(1969) 107
[3] G. Parthasarathy and E. S. R. Gopal, Bull. Mater. Sci. 3&4 (1985) 271
[4] R. Zallen, B.A. Weinstein and M. L. Slade, J. Phys. 42(1981) C4-241; B.A. Weinstein, R. Zallen, M.L. Slade and J. C. Mikkelsen Jr., Phys. Rev. B 25(1982) 781

[5] Y. Kawamoto and S. Tsuchihashi, J. Am. Ceram. Soc. 52 (1961) 626; 54 (1971) 131
[6] Y. Xu and W. Y. Ching, Phys. Rev. B44 (1991) 11048
[7] S. I. Zabinsky, J. J. Rehr, A. Ankudinov, R. C. Albers and M. J. Eller, Phys. Rev. B52 (1995) 2995

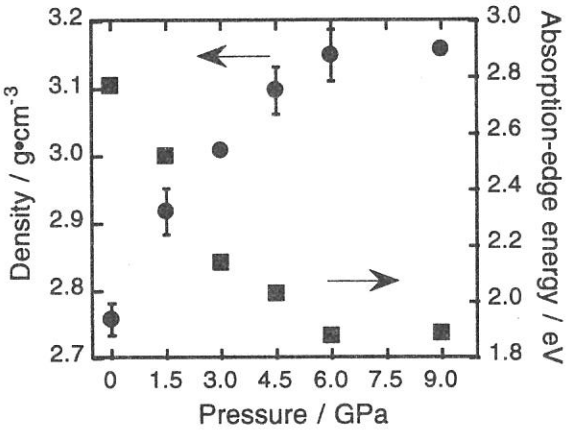

Fig. 1. Pressure dependence on density (●) and absorption-edge energy in visible region (■) in undensified and densified GeS_2 glasses.

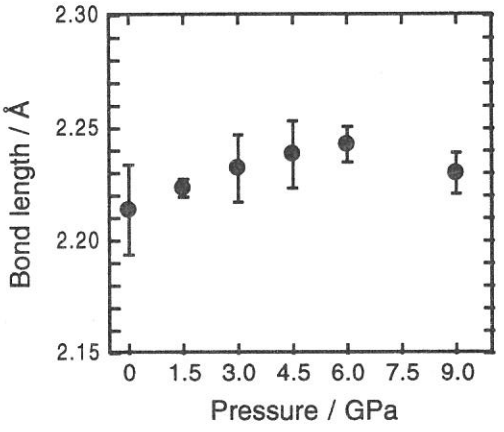

Fig. 2. Pressure dependence of S-Ge bond length in undensified and densified GeS_2 glasses.

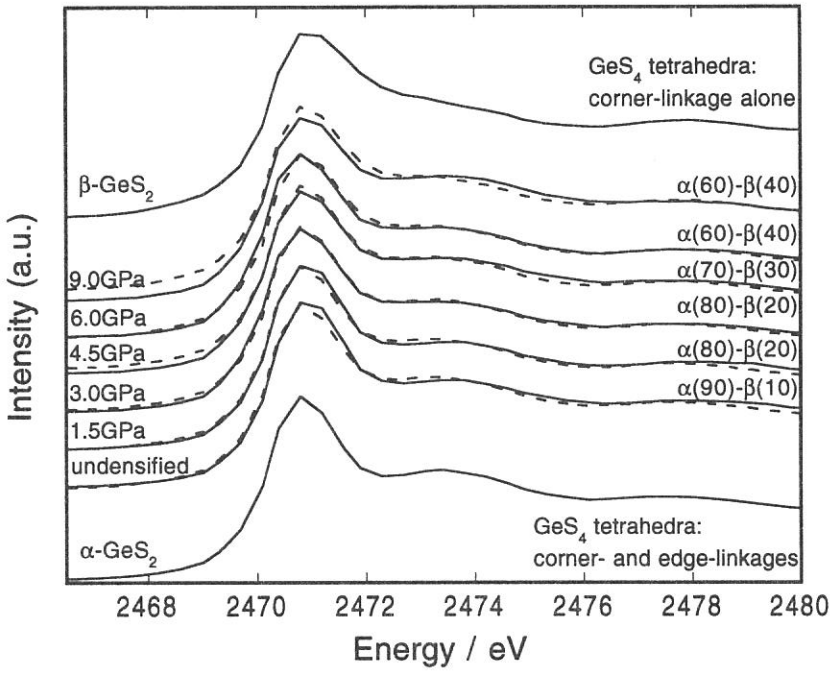

Fig. 3. Pressure dependence of S-K XANES spectra of undesified and densified GeS_2 glasses. (solid line: experimental, dashed line: simulated)

(BL7A)

Crystalline structure of impurity-doped multinaly compound semiconductor

Tooru Tanaka, Qixin Guo*, and Akihiro Wakahara

Department of Electrical and Electronic Engineering, Toyohashi University of Technology, Toyohashi 441-8580, Japan

**Department of Electrical and Electronic Engineering, Saga University, Saga 840-8502, Japan*

I -III-VI_2 chalcopyrite semiconductors, such as $CuInSe_2$ and $Cu(In,Ga)Se_2$, have been one of the leading candidates for absorbers in hetero-junction photovoltaic devices because of their direct bandgap and high absorption coefficient[1]. These devices have been demonstrated to exhibit high conversion efficiency close to 19%[2].

The electrical properties, both the conductivity type and the carrier concentration, of $CuInSe_2$ strongly depend on the Cu/In and Se/(Cu+In) compositional ratio. $CuInSe_2$ thin films for high efficiency solar cells are fabricated by co-evaporation technique with precise control of the Cu/In ratio. In order to achieve a solar cell with higher efficiency and larger area, it is important to establish the doping technique using extrinsic dopants. However, the detailed roles of doped impurity in $CuInSe_2$ have not yet been clarified.

Recently, We have investigated the effect of implanted Mg on the electrical properties of $CuInSe_2$ epitaxial films[3]. It was found that Mg atoms act as donor in $CuInSe_2$, and that the electron concentration increased linearly with increasing the Mg concentration in the films. However, the concentration ratio of the implanted Mg to carrier electron at room temperature was as low as about 1%, and thus, all of the Mg atoms seem not necessarily to be present on donor site. As the next step, we should clarify the doping mechanism by Mg in $CuInSe_2$. In this work, we measured Mg K-edge XANES spectra of Mg-implanted $CuInSe_2$ thin films in order to investigate the local structure around Mg atoms.

Epitaxial $CuInSe_2$ thin films were grown on semi-insulating GaAs(001) substrate at the substrates temperature of 450℃ for 180min by RF diode sputtering. Mg atoms were implanted into the films at room temperature using three kinds of accelerating energies, 60, 140, and 200keV, in order to fabricate the box profile of Mg atoms within a depth of 300nm from the surface. The mean Mg concentration in the implanted layer of the films used in this measurements were $5\times10^{19}cm^{-3}$ and $5\times10^{20}cm^{-3}$. After implantation, the films were annealed at 400℃ for 60min in N_2 atmosphere to eliminate implantation damage, and activate Mg atoms electrically.

Soft X-ray absorption experiments were carried out on the beam line BL7A station at the Ultraviolet Synchrotron Radiation Facility (UVSOR) in the Institute for Molecular Science, Okazaki, Japan, with a ring energy 750MeV and stored current of 80-200mA. Mg K-edge X-ray absorption spectra were recorded using a beryl two-crystal monochromator. Data were collected in a total electron

yield mode under high vacuum (<10^{-7}Torr) at room temperature. The samples were put on the first photocathode made of Cu-Be of the electron multiplier by using adhesive carbon tape.

Figure 1 shows Mg K-edge XANES spectra of Mg-implanted $CuInSe_2$ thin. We have obtained clear XANES spectra. By analyzing the spectra, local structure around Mg atoms would be characterized, and it has been now in progress.

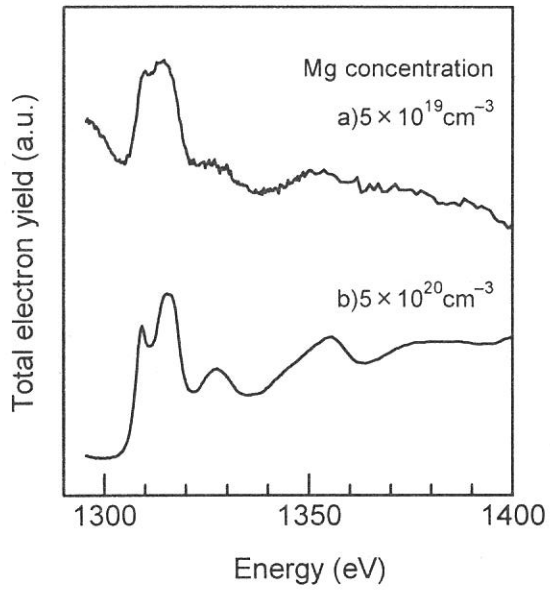

Fig.1 Mg K-edge XANES spectra of Mg-implanted $CuInSe_2$ films with a mean Mg concentration of (a)$5\times10^{19}cm^{-3}$ and (b)$5\times10^{20}cm^{-3}$.

Acknowledgements

The authors would like to thank Professor T.Kinoshita and other staff members of the UVSOR facility for the useful advice and technical support. We are also grateful to Mr. H.Sato and Mr. M.Nakajima for their help in the experiment.

References

[1] D.Haneman, Crit. Rev. Solid State Mater. Sci. **14,** 377 (1988).
[2] M.A.Contreras, B.Egaas, K.Ramanathan, J.Hiltner, A.Swartzlander, F.Hasoon, R.Noufi, Progress in Photovoltaics, **7**, 311 (1999).
[3] T.Tanaka, A.Wakahara, A.Yoshida, T.Ohshima, H.Itoh, and S.Okada, J.Appl.Phys. (in press).

(BL7A)

Al K-edge study for Al doped Lithium Manganese Spinel Oxides for Lithium Secondary Batteries

Yoshiharu UCHIMOTO, Takeshi YAO, and Taiji SASADA
Department of Fundamental Energy Science,
Graduate School of Energy Science, Kyoto University,
Yoshida, Sakyo-ku, Kyoto 606-8501, JAPAN

Secondary lithium batteries using intercalation compounds as the cathode active material have been studied intensively. Among many intercalation compounds, $LiMn_2O_4$ based spinel type oxides are one of the most promising cathode materials used in lithium ion batteries because their low cost, high theoretical energy density. (1-5) However the capacity of the battery using $LiMn_2O_4$ fades out during charge-discharge cycling at around 4 V. Recently, Al doped $LiMn_2O_4$ material have shown better cycle performance at around 4 V compared with the cycleability of undoped $LiMn_2O_4$. (6-7)

The unit cell of the ideal spinel structure (space group: *Fd3m*) is given in Fig. 1. In this ideal structure, oxide ions form a cubic close packing, in which cations partly occupied tetrahedral and octahedral interstices. The unit cell of $LiMn_2O_4$ contains 56 atoms; 32 O, 16 Mn, and 8 Li. The oxide ions occupied 32e position, lithium ions occupied tetrahedral 8a positions, and manganese ions occupied octahedral 16d positions. In order to understand the improvement of cycleability by Al doping, it is important to clarify doping site of Al cations on the cubic spinel structure. In the present study, Al cation doped spinels ($LiAl_xMn_{1-x}O_4$) were prepared. X-ray diffraction (XRD), X-ray Absorption Fine Structure (XAFS), and electrochemical studies were carried out. Especially, Al K-edge X-ray Absorption Near Edge Structure (XANES) analysis was used to determine the Al doping site; 16d (octahedral position) or 8a (tetrahedral position).

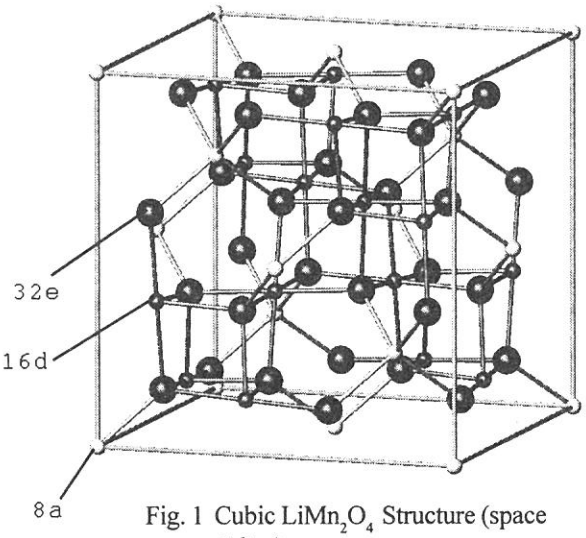

Fig. 1 Cubic $LiMn_2O_4$ Structure (space group *Fd3m*).

$LiAl_xMn_{1-x}O_4$ spinels were prepared from lithium carbonate, manganese carbonate, and aluminium hydrate. The mixture was calcined for 48 hours at 850°C. The crystal structure of the product was determined by XRD using MoKα radiation. Fig. 1 shows XRD pattern of $LiAl_xMn_{1-x}O_4$. The $LiAl_xMn_{1-x}O_4$ (x=0.0, 0.05, 0.1, 0.2) were indexed to an cubic lattice. Above x=0.3, unknown peaks appeared. The lattice parameters and other

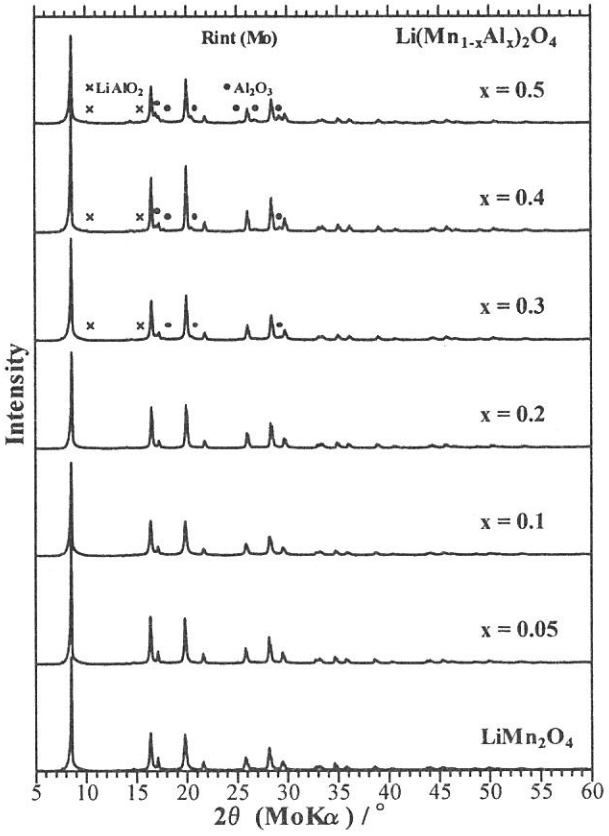

Fig. 2 XRD pattern of $LiAl_xMn_{1-x}O_4$

structural parameters for samples below x=0.2 were refined by the Rietveld method. The Rietveld analysis was confirmed that the samples were belonging to cubic *Fd3m* space group.

Al K-edge XANES spectra were measured at room temperature in a total electron yield mode at BL-7A at UVSOR line with two quartz crystals. The Al K-edge XANES spectra were powerful tool to determine the coordination number of Al cations. (8-10) Fig. 3 shows a Al K-edge XANES of $AlPO_4$ and Al_2O_3. In the $AlPO_4$, AlO_4 (tetrahedra) is dominant, whereas in the Al_2O_3, AlO_6(octahedra) is dominant.

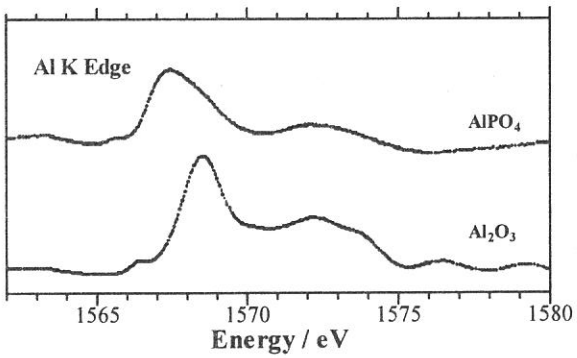

Fig. 3 Al K-edge XANES of $AlPO_4$ and Al_2O_3.

Fig. 4 shows Al K-edge XANES of $LiAl_xMn_{1-x}O_4$ (x = 0.0, 0.05, 0.075, 0.1, 0.2, 0.3, 0.4, and 0.5) together with those of reference compounds of $AlPO_4$ (AlO_4 :tetrahedra) and Al_2O_3 (AlO_6 :octahedra). The figure clearly indicates that the AlO_6 octahedra is predominant for $LiAl_xMn_{1-x}O_4$ (x=0.0, 0.05, 0.1, 0.2) which were belonging to cubic *Fd3m* space group. This means that Al doping site is mainly 16d (octahedral position) in the cubic spinel structure. From the data of the standard Gibbs energy of the information of Al_2O_3 and Mn_2O_3, the Al-O bond is stronger than Mn-O bond in the octahedra. (6) The M-O bond at 16d (octahedral position) in the cubic spinel structure are stronger by Al doping, so that the Al doping improve the cycleability of the lithium secondary battery.

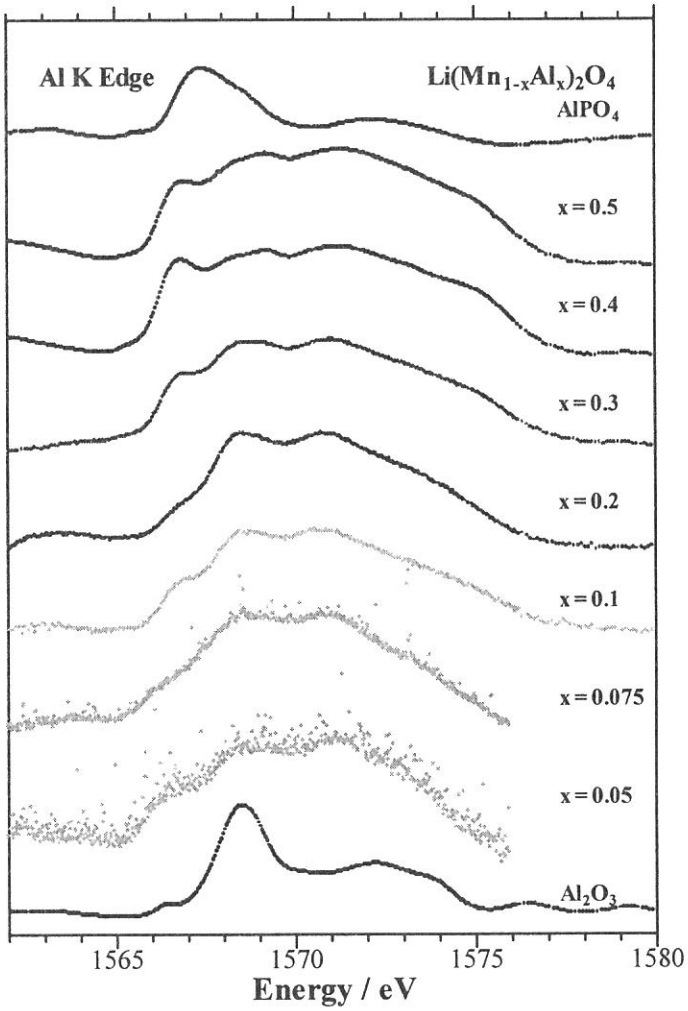

Fig. 4 Al K-edge XANES of $LiAl_xMn_{1-x}O_4$ (x = 0.0, 0.05, 0.075, 0.1, 0.2, 0.3, 0.4, and 0.5) together with those of reference compounds of $AlPO_4$ and Al_2O_3.

REFERENCES

1) D. Guyomard, J.M. Tarascon, *Solid State Ionics*, **69**, 222 (1996).
2) W. Liu, G.C. Farrington, F. Chaput, and B. Dunn, *J. Electrochem. Soc.*, **143**, 879 (1996).
3) Y. Xia, H. Takeshige, H. Noguchi, and M. Yoshio, *J. Power Sources*, **56**, 61 (1995).
4) H. Ohzuku, M. Kitagawa, T. Hirai, *J. Electrochem. Soc.*, **137**, 769 (1990).
5) K. Kanamura, H. Naito, T. Yao, and Z. Takehara, *J. Mater. Chem.*, **6**, 33 (1996).
6) D. Song, H. Ikuta, T. Uchida, and M. Wakihara, *Solid State Ionics*, **117**, 151 (1999).
7) F. Le Cras, D. Bloch, M. Anne, and P. Strobel, *Solid State Ionics*, **89**, 203 (1996).
8) G.A. Waychnas and G.E. Brown Jr., *EXAFS and Near Edge Structure III*, Springer-Verlag, Berlin, 336 (1984).
9) J. Wong, Z.U. Rek, M. Rowen, T. Tanaka, F. Schafers, B. Muller, G.N. George, I.J. Pickering, G. Via, B. DeVries, G.E. Brown Jr, M. Froba, *Physica B*, **208&209**, 220 (1995).
10) K. Shimizu, Y. Kato, T. Yoshida, H. Yoshida, A. Satsuma, and T. Hattori, *UVSOR Activity Report*, 174 (1998).

(BL-7A)

XAFS study on Al coordinations in silica-alumina prepared by sol-gel method

Hisao Yoshida,[a] Norimitsu Matsushita,[a] Yuko Kato,[a] Ken-ichi Shimizu,[a] Tomoko Yoshida[b] and Tadashi Hattori[a]

[a] *Department of Applied Chemistry, Graduate School of Engineering, Nagoya University, Nagoya, 464-8603, Japan*

[b] *Center for Integrated Research in Science and Engineering, Nagoya University, Nagoya, 464-8603, Japan*

Abstract

By means of Al K-edge XANES study at UVSOR, it was clarified that the AlO_4 species in silica-alumina catalysts were responsible for their activity in photoinduced non-oxidative methane coupling at room temperature.

Introduction

In order to convert natural gas into useful chemicals, the oxidative methane coupling is an expedient reaction. However, it is quite difficult to obtain the coupling products in high selectivity, because the oxidation of coupling products to CO_x proceeds more selectively than the coupling reaction. When the oxidant molecules are removed to avoid the complete oxidation, the reaction should require very high temperature [1]. Recently, photoinduced non-oxidative methane coupling was found to proceed on silica-alumina in yields as high as 5 % without formation of CO and CO_2 [2]. The active sites on silica-alumina were proposed to be the highly dispersed Al species in the silica matrix. In the present study, we focussed the coordination states of Al species in the silica-alumina prepared by sol-gel method and their photoactivity.

Experimental

The samples of silica-alumina were prepared by sol-gel method. After a mixture of $Si(OEt)_4$ and ethanol (mol ratio, 1/5) was stirred for 1 h, another mixture of ethanol, distilled water, $Al(NO_3)_3$ and nitric acid (mol ratio, 5/50/x/0.02, x=0.02-2) was added dropwise, followed by stirring for 1 h. Dehydration proceeded at 353 K with suction. When geration started, the mixture was dried without stirring, followed by drying at 383 K for 12 h, grind and calcination in a flow of dry air (60 ml/min) at 773 K for 5 h to obtain the silica-alumina powder samples. Pure silica sample was prepared from $Si(OEt)_4$ by sol gel method in water-ethanol mixture at boiling point followed by grind and calcination. Pure alumina was prepared by calcination of $Al(NO_3)_3$. They were stored under ca. 80% humidity at room temperature.

Before the reaction test, the sample was heated in air up to 1073 K and then evacuated. Subsequently the sample were treated with 100 Torr oxygen (1 Torr=133.3 Nm^{-2}) at 1073 K for 1 h, followed by evacuation at the same temperature for 1 h. The reaction test was carried out under irradiation by using a 250 W Xe lamp for 6 h. No oxidant molecules was introduced into the reaction system. Under photoirradiation, the temperature of sample bed was measured to be around 310 K. Products in the gaseous phase were collected with a liquid-N_2 trap and analyzed by GC. BET specific surface area of the samples was measured after the reaction test.

Soft X-ray absorption experiments were carried out on the beam line 7A [3] at UVSOR, Institute for Molecular Science, Okazaki, Japan, with a ring energy 750 MeV and stored current of 130-200 mA. Two-crystals monochromator employing YB_{66} crystals were used for recording Al K-edge XAFS [4]. Data were collected in a total electron yield mode under high vacuum (residual pressure $<1\times10^{-6}$ Torr) at room temperature. The sample was put on the first Cu-Be dynode of the electron multiplier (-1.5 kV) by using adhesive carbon tape.

Table 1 Results of characterization and ethane yield in photoinduced non-oxidative methane coupling

Al composition (Al/(Si+Al)%) [a]	BET surface area (m^2g^{-1}) [b]	ethane yield (%) [c]	ethane yield per surface area ($x10^{-4}$ % /m^2g^{-1}) [c/b]	ethane yield per amount of surface Al ($x10^{-4}$ %/m^2g^{-1}/atom%) [c/b/a]
0.0	297	0.022	0.75	-
2.0	137	0.067	4.9	2.4
9.1	258	0.058	2.8	0.58
16.7	273	0.104	3.8	0.22
37.5	203	0.091	4.5	0.12
50.0	98	0.041	4.8	0.096
66.7	93	0.051	5.5	0.083
100	92	0.049	5.3	0.053

Results and discussion

The Al in the each silica-alumina sample prepared was confirmed to be homogeneously dispersed in bulk and surface since the surface Al concentration estimated by XPS was in good agreement with the bulk composition. The BET surface area of the samples containing Al of more than 50 % was obviously smaller than those of low Al content samples as shown in Table 1.

In the photoinduced non-oxidative methane coupling, only ethane was obtained as gaseous product in this condition. The ethane yield listed in Table 1 did not show a linear correlation with Al composition, which should be affected by the differences of specific surface area and Al composition. The activity normalized by them (the last column in Table 1) shows good relation to the Al composition; the lower Al composition sample exhibited the higher activity. It supports the proposal that highly dispersed Al species in silica-alumina would be active sites [2].

Fig. 1 shows the normalized Al K-edge XANES spectra of silica-alumina and alumina samples together with those of model compounds containing AlO_4 tetrahedra (mordenite) and AlO_6 octahedra (corundum) [5]. The spectra of the silica-alumina samples varied with their Al contents (Fig. 1 a-f). The low Al content samples (Fig. 1a, b) show a peak at around 1566 eV, which is assigned AlO_4 species as shown in the spectrum of mordenite (Fig. 1h). This peak broadened to higher energy and a broad peak at around 1572 eV became apparent as increase of Al contents (Fig. 1c-f). The alumina sample showed the obvious peaks at 1568 eV and 1572 eV(Fig. 1g). The peaks at 1568 and 1572 eV are assigned to AlO_6 species as shown in the spectrum of the corundum alumina (Fig. 1i). These results indicate that the fraction of AlO_6 species in the silica-alumina samples increased as increase of Al contents. In the other words, AlO_4 species are predominant in the lower Al content samples.The activity in photoinduced non-oxidative methane coupling to produce ethane mentioned above also showed the same tendency.

As a conclusion, it was claimed that the activity of the silica-alumina samples in this photoreaction would be responsible for the surface AlO_4 species.

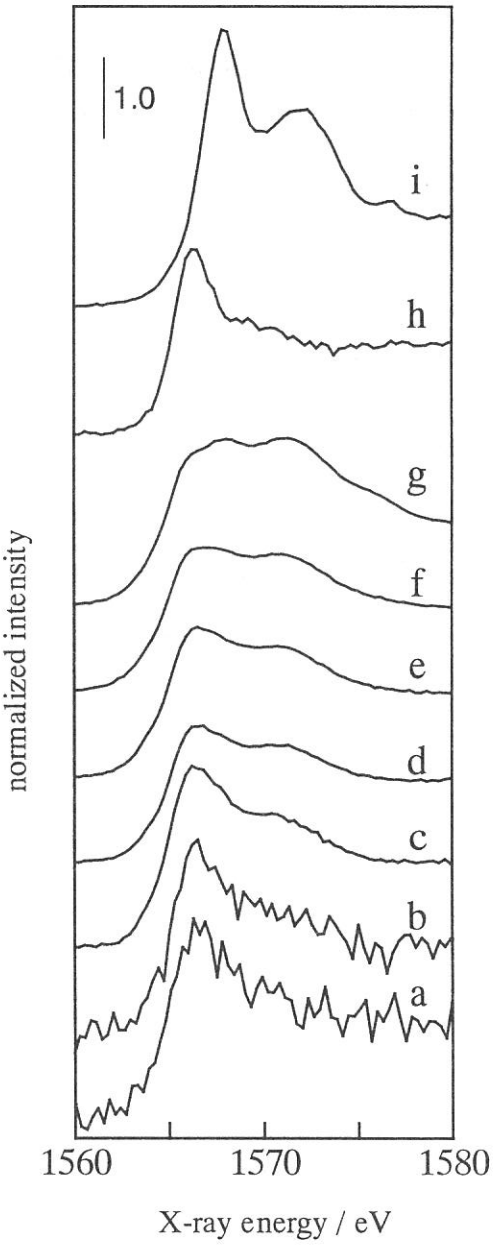

Fig. 1 Al K-edge XANES spectra of silica-alumina samples whose Al contents (mol%) of 2.0 (a), 9.1 (b), 16.7 (c), 37.5 (d), 50 (e) and 66.7 (f), and alumina calcined at 773 K (g), mordenite-type zeolite (JRC-Z-HM15, tetrahedral) (h) and alumina (corundum, octahedral) (i).

References

1. L. Guczi, R. A. Van Santen and K. V. Sarma, *Catal. Rev. Sci.-Eng.*, 38 (1996) 249.
2. Y. Kato, H. Yoshida and T. Hattori, *Chem. Commun.*, 1998, 2389.
3. T. Murata, T. Matsukawa, S. Naoe, T. Horigome, O. Matsudo and M. Watanabe, *Rev. Sci. Instrum.* 63 (1992) 1309.
4. T. Kinoshita, Y. Takata, T. Matsukawa, H. Aritani, S. Matsuo, T. Yamamoto, M. Takahashi, H. Yoshida, T. Yoshida, Y. Ufuktepe, K. G. Nath, S. Kimura, H. Kumigashira and Y. Kitajima, *J. Synchrotron Rad.*, 5 (1998) 726.
5. K. Shimizu, Y. Kato, T. Yoshida, H. Yoshida, A. Satsuma and T. Hattori, *Chem. Commun.*, (1996) 1681.

(BL 7A)

Study on D^+ irradiated Si surface by XAFS

Tomoko Yoshida,[a*] Hisao Yoshida,[b] Takanobu Hara,[c] Mikio Sakai[c] and Tetsuo Tanabe[a]

[a] *Center for Integrated Research in Science and Engineering, Nagoya University, Nagoya 464-8603, Japan*

[b] *Department of Applied Chemistry, Graduate School of Engineering, Nagoya University, Nagoya 464-8603, Japan*

[c] *Department of Nuclear Engineering, Graduate School of Engineering, Nagoya University, Nagoya 464-8603, Japan*

Introduction

Ion implantation is commonly used as a method to modify the near-surface properties of materials. By controlling the fluence and energy of incident ions, one can introduce the desired amount of foreign species into suitable depth in host materials. Simultaneously the kinetic energy of implanted ions introduces lattice damage through electron excitation and atomic displacement processes, sometimes resulting in undesirable modification of the near-surface structure. Therefore characterization of the implanted materials with fine depth resolution is a very important task. In the present work, we have applied an X-ray absorption technique for characterization of silicon samples implanted by deuterium with the difference in the depth distribution of implanted deuterium and produced damages.

Experimental

Deuterium ion irradiation was carried out in a standard vacuum chamber equipped with an ion source at room temperature[1]. With an aid of differential pumping system, the pressure of the target chamber was kept below 10^{-8} Torr during the irradiation. Mass analyzed deuterium ions (D^+) accelerated up to 5 keV were injected into a Si target (100) through a slit of 5 mm diameter with an incident angle of 22.5 degrees with respect to the target normal. Since the samples were stored in air, they were exposed to atmospheric oxygen.

Si K-edge XANES spectra were recorded under vacuum ($<10^{-7}$ Torr) at room temperature at the beam line 7A station attached with a two-crystal InSb monochromator at UVSOR, Institute for Molecular Science, Okazaki, Japan. The ring energy was 750 MeV and stored current was 100-200 mA during measurement. The sample was directly put on the first photocathode made of Cu-Be of the electron multiplier with the voltage of - 1.5 keV. Data were collected in a total electron yield mode, in which X-ray energy dependence of Si KLL Auger electron yield is mainly monitored.

Results and Discussion

Fig. 1 shows Si K-edge XANES spectra of unirradiated silicon (a) and deuterium irradiated silicons with incident energy of 5 keV (b-d). The XANES spectrum of a pure silica glass is also shown in Fig. 1 (e) as a reference. The features of the XANES spectrum changed with increase of D^+ ion fluence. After the irradiation of 1.6×10^{18} ions/cm^2, characteristic peaks of unirradiated silicon disappeared (Fig. 1 (b)), indicating that the regular tetrahedral structure of silicon was disordered by D^+ ion bombardment. In this spectrum, a pronounced peak at around 8 eV was also appreciable. Since the energy position of the peak agreed with that of the large characteristic peak of silica (Fig. 1 (e)), this result clearly indicates that the target surface was oxidized to SiO_2. As shown in Fig. 1(a), the peak corresponding to SiO_2 was not observed for the XANES spectrum of unirradiated silicon. Accordingly, the appearance of SiO_2 species can be regarded as an indication of displacement of surface silicon atoms, which easily attract or bind oxygen in residual gas during the irradiation and/or in atmosphere during the transfer for the XAFS measurements.

In addition to the surface oxidation, as shown in Fig. 1 (c, d), when D^+ ion fluence was over ca. 2×10^{18} ions/cm^2, a remarkable change was observed in the XANES spectra. This strongly indicates that the electronic and atomic structures of these samples changed to others from those of a pure silicon, i.e., such a change is much considerable compared with the merely disordering of the regular tetrahedral structure of silicon as shown in Fig. 1 (b). Since the edge due to Si(0) state almost disappeared and simultaneously a sharp peak was observed at around 5 eV, it is likely that most Si(0) atoms changed to new Si species which are in higher valence states by the irradiation. On the basis of the energy position of the new peak, they must be in the intermediate states between Si(0) and Si(4+). However, less valenced silicon oxide like SiO is known to be unstable.[2] Therefore the new Si species should correspond to Si-D (SiDn species) formation with implanted deuterium as follows. As mentioned above, under irradiation at 5 keV, the amount of implanted deuterium is less than the number of the displaced atoms. Accordingly the peak due to the Si-D formation appeared after the deuterium irradiation over 2×10^{18} ions/cm^2, whereas the peak due to SiO_2 was clearly observed for the irradiation of 1.6×10^{18} ions/cm^2. Rather drastic structural change as observed between Fig. 1 (b) and Fig. 1 (c) would indicate abrupt formation of SiDn local structure after the implantation of a certain amount of deuterium ions. The formation of the SiHn species in which Si ions are in the intermediate states between Si(0) and Si(4+) has been reported to occur by the assist of the bubble or crack formation under hydrogen irradiation.[3,4]

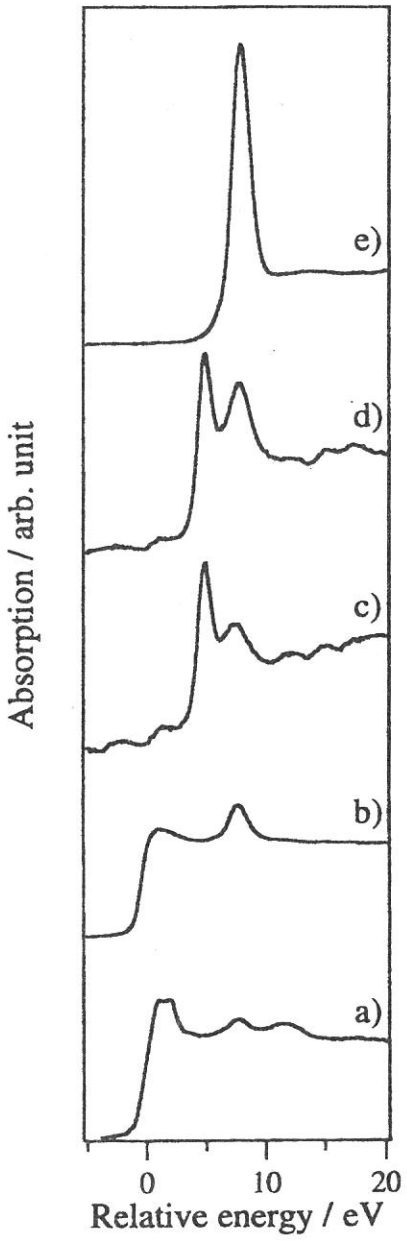

Figure 1
Si K-edge XANES spectra of a) unirradiated silicon, b-d) silicon samples irradiated by 5 keV deuterium ions, and e) a silica sample. The fluence of deuterium ions is b) 1.6×10^{18} / cm^2, c) 2.1×10^{18} / cm^2 and d) 2.9×10^{18} / cm^2. Energy offset is taken to be 1838 eV.

References

1) Tanabe, T., Tanaka, S., Yamaguchi, K., Otsuki, N., Iida, T., and Yamawaki, M. (1994) *J. Nucl. Mater.* **212-215**, 1050.
2) Yamamoto, H., Baba, Y., Sasaki, T. A. (1995). *Surf. Interf. Anal.* **23**, 381.
3) Doyle, B. L. (1982). *J. Nucl. Mater.* **111-112**, 628.
4) Varma, C. M. (1997) *Appl. Phys. Lett.* **71**, 3519-3521.

(BL8B1)

C K-edge XANES of Carbonaceous Materials on Catalysts

T. Shishido,[a] M. Kondo, H. Sameshima,[a] S. Takenaka,[b] and K. Takehira[a]

[a] *Department of Applied Chemistry, Faculty of Engineering, Hiroshima University, Kagamiyama 1-4-1, Higashi-hiroshima, Hiroshima 739-8527, Japan*

[b] *Department of Applied Chemistry, Graduate School of Engineering,, Tokyo Institute Technology, Ookayama, Meguro-ku, Tokyo 152-8522, Japan*

Introduction

In recent years, carbon fibers grown over metal species such as Fe, Co, Ni from the decomposition of hydrocarbons have been interesting materials [1-3]. Several novel carbon structures such as fullerens and nanotubes have been formed in similar systems, and bringing excitement to many fibers [4-6], due to their extraordinary physical and chemical properties. Efforts have been made to control the morphology and size of the nanotubes (or fibers) and to improve the efficiency of the production processes. It has been proposed that the growth process was composed of several steps such as adsorption, bulk diffusion, and formation of fibers. It has also proposed that the deactivations of metal species occur due to encapsulation by a graphite layer [2]. These results indicate that the catalytic activities of metal species strongly depend on the structure of carbonaceous materials.

The metal (Ni, Fe and Co) supported catalysts were prepared and testes for the methane decomposition at a high temperature. In this report, we attempted to characterize the structures of carbonaceous materials on the metal (Ni, Fe, Co) supported catalysts by means of C K-edge XANES spectroscopy.

Experimental

The metal supported catalysts were prepared by conventional impregnation method. The catalytic activity for decomposition of methane was carried out using a conventional flow system. The C K-edge XANES spectra of the catalysts were collected at room temperature in a total electron yield mode at BL-8B1 at UVSOR. In most part of experiments, the sample was put on a carbon tape and then the carbon tape was put on a Cu-Be dinode which is attached to the first position of the electron multiplier.

Results and Discussion

The C K-edge XANES spectra of the 5wt% metal/γ-Al_2O_3 catalysts used for methane decomposition at 900°C are shown in Figure 1. Figure 2 shows the C K-edge XANES spectra of 5wt% Ni/SiO_2 and Ni/MgO catalysts used for methane decomposition together with carbon tape. The shapes of the XANES spectra were almost same, regardless of kind of metal and support of the catalysts, suggesting that the

structures of the carbonaceous materials formed during the decomposition of methane on all the catalyst are almost same. In the C K-edge XANES spectra of all the catalysts, the band at 285eV and broad band between 290eV and 315eV could be confirmed. In general, the band at 285eV is assigned to $1s \rightarrow \pi^*$ resonance and the broad band around 300eV is assigned to $1s \rightarrow \sigma^*$. The negative band at 288ev was also observed in the C K-edge XANES spectra of all the catalysts. In this peak position, a sharp band was observed in the C-K-edge XANES spectrum of carbon tape, suggesting that the background subtraction is inappropriate in this energy region. In order to collect clear C K-edge XANES spectra, another method for background subtraction should be needed.

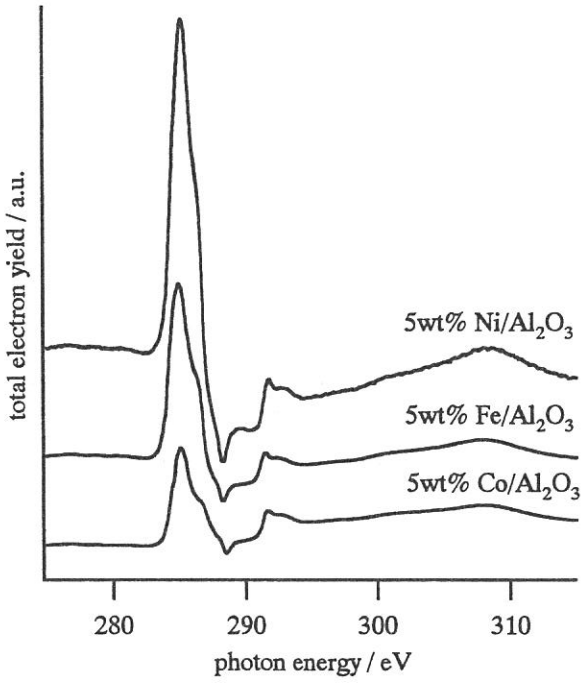

Figure 1 CK-edge XANES spectra of metal/Al_2O_3 catalysts

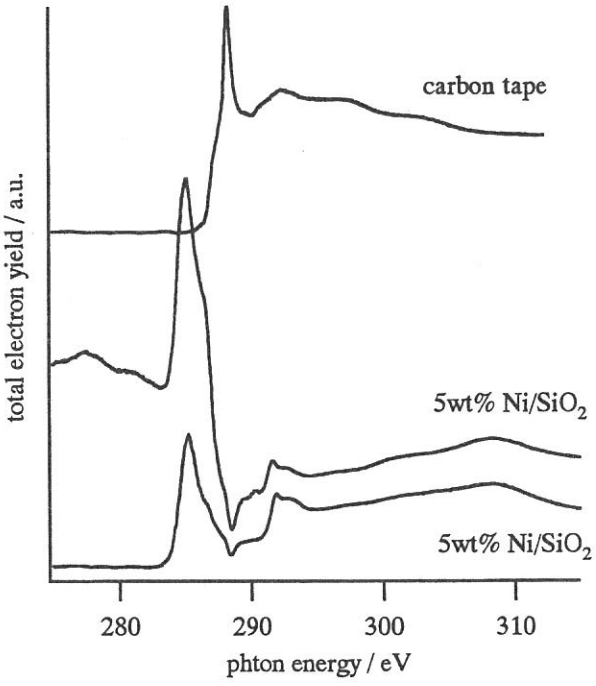

Figure 2 CK-edge XANES spectra of Ni/MgO and Ni/SiO_2 catalysts

References

[1] M. Endo, *Chemtech*, **Sept.**, 568 (1988).

[2] R. T. K. Baker, *Carbon*, **27**, 315 (1989).

[3] M. N. Rodriguez, *J. Mater. Res.*, **8**, 3233 (1993).

[4] S. Iijima, *Nature*, **354**, 56 (1991).

[5] T. W. Ebbesen, and P. M. Ajayan, *Nature*, **358**, 220 (1992).

[6] J. H. Weaver, *Science*, **265**, 611 (1994).

(BL8B1)

Electronic Structure in $Li_{1\pm x}Mn_2O_4$ Spinel Oxides from Mn *L*-edge and O K-edge XANES

Yoshiharu UCHIMOTO, Takeshi YAO, and Taiji SASADA
Department of Fundamental Energy Science,
Graduate School of Energy Science, Kyoto University,
Yoshida, Sakyo-ku, Kyoto 606-8501, JAPAN

$LiMn_2O_4$ based spinel type oxides are one of the most promising cathode materials used in lithium ion batteries because their low cost, high theoretical energy density. (1, 2) It is important to clarify the change of electronic structure during charge and discharge process in order to understand their electrochemical properties. In this study, the electronic structure of $LiMn_2O_4$ spinel oxide was determined by using a measurement of Mn L_{23}-edge and Oxygen K-edge X-ray Absorption Near Edge Structure (XANES). XANES spectra were measured on BL-8B1 at UVSOR with ring energy of 750 MeV in a mode of total electron yield.

$LiMn_2O_4$ spinel was prepared from lithium carbonate and manganese carbonate. The lithium carbonate and manganese carbonate were weighted with molar ratio as Li:Mn=1:2 and mixed for 5h. The mixture was pressed into disk and heated at 850°C for 48 hours. The crystal structure of the oxide was determined by XRD using MoKα radiation. These XRD patterns were indexed to a cubic lattice. The lattice parameters and other structural parameters were refined by the Rietveld method. The Rietveld calculation was performed on the vector processor (Cray Y-MP2E/264) at the Institute for Chemical Research, Kyoto University, by using 'Rievec' computer program (3, 4) Fig. 1 shows the results of the Rietveld analysis. The observed pattern agreed well with the calculated pattern. The obtained lattice parameters are given in Table 1. R_{wp}, R_F, and R_B are small enough to guarantee the reliability, and it was confirmed that $LiMn_2O_4$ is belonging to cubic *Fd3m* space group.

Figure 2 shows a low rate discharge curve of $LiMn_2O_4$ spinel. The $LiMn_2O_4$ spinel shows mainly 2 different plateau regions of a voltage range of 3.8-4.1 V and a voltage range of 2.8 V. XANES analysis were performed to clarify the oxidation

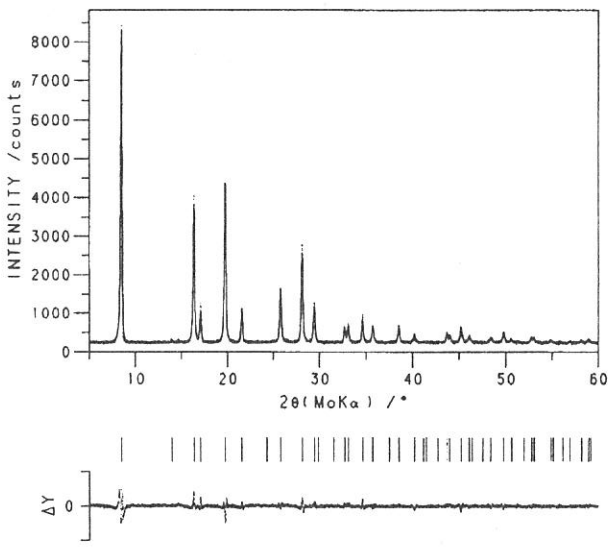

Cubic Spinel
Space group : *Fd3m*

Atom	site	x	y	z
Li	8a	0	0	0
Mn	16d	0.625	0.625	0.625
O	32e	0.3866(1)	0.3866(1)	0.3866(1)

a = 8.24941(4) Å

R_{wp}, R_F, R_B = 0.0699,0.0340,0.0306

Fig. 1 The result of Rietveld analysis of $LiMn_2O_4$ .The observed and calculated XRD patterns are indicated by dots and solid, respectively. The differnce between observed snd calculated is plotted below.

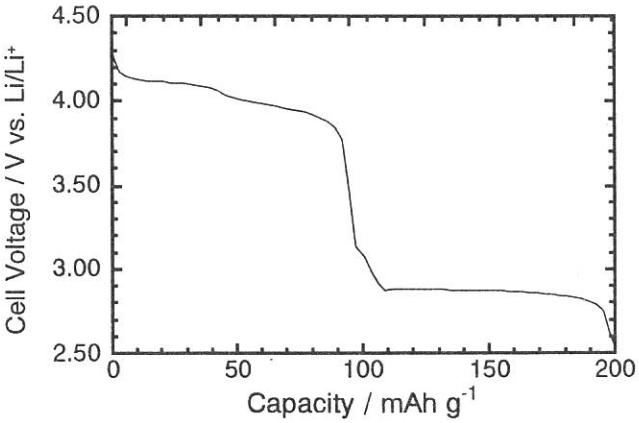

Fig. 2 Voltage versus capacity for $LiMn_2O_4$.The cell was cycled between 4.3V and 2.5V at 0.1mA / cm^2.

state of manganese and nickel for various x values in $LiMn_2O_4$ spinel.

Fig. 3 shows the Mn L-edge XANES of $Li_xMn_2O_4$ at various x values together with reference materials of MnO_2 (Mn^{4+}), Mn_2O_3 (Mn^{3+}), and $MnCO_3$ (Mn^{2+}). The spectra correspond to $Mn2p^63d^n$ to $Mn2p^53d^{n+1}$ transitions. This figure shows that the Mn L_3 absorption edge of Mn_2O_3 was about 642.0 eV and that of MnO_2 was 643.4 eV. These results indicate that increasing the oxidation state of manganese, the Mn L_3 absorption edge shifted to higher energy. As shown in Fig. 3, the peak of $LiMn_2O_4$ was a combination of peak of Mn_2O_3 and MnO_2. At low x value of the $Li_xMn_2O_4$, contribution of Mn^{4+} increased, whereas contribution of Mn^{3+} increased at large x values.

Fig. 4 shows the oxygen K-edge XANES of $Li_xMn_2O_4$ at various x. A peak at about 529 eV is attributed to the band derived from the mixing of the Mn 3d majority (spin-up) e_g and minority (spin-down) t_{2g} states with oxygen 2p states. A peak at about 531.5 eV is attributed to the band derived from the mixing of the Mn 3d minority (spin-down) e_g states with oxygen 2p states. The broad structure about 540-545 eV is attributed to band of Mn 4sp character. The peak at about 529 eV increased with decreasing lithium content. This results shows that oxidation also take place on oxygen 2p orbital and the ground state of $Li_xMn_2O_4$ ($x<1.0$) is mixed state of $3d^3$ and $3d^4L$, where L represents a ligand hole state. These results are in good agreement with the result of First-Principles calculation for $LiMn_2O_4$ spinel oxides. (5, 6) At x values above 1.2, the peak at about 534 eV appeared. The peak at about 534 eV is attributed to minority (spin-down) d_{x2-y2} state, which appeared by cubic-to-tetragonal phase transition.

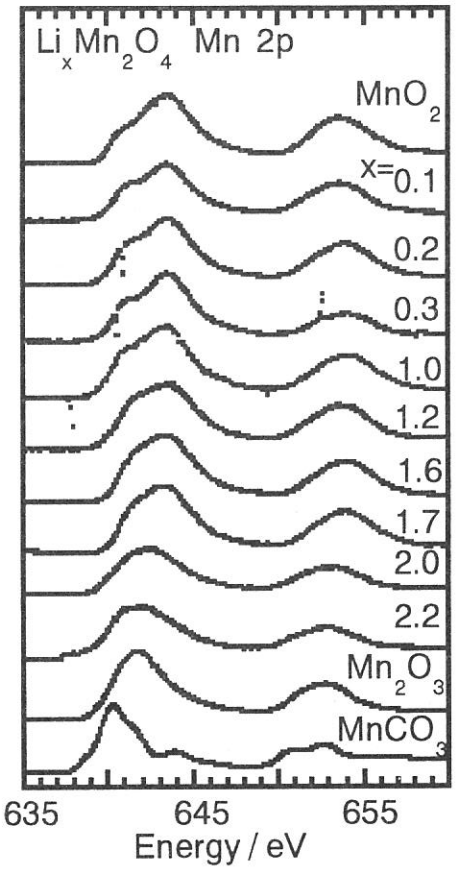

Fig.3 Mn 2p absorption spectra of $Li_xMn_2O_4$, the value of x is indicated in the figure.

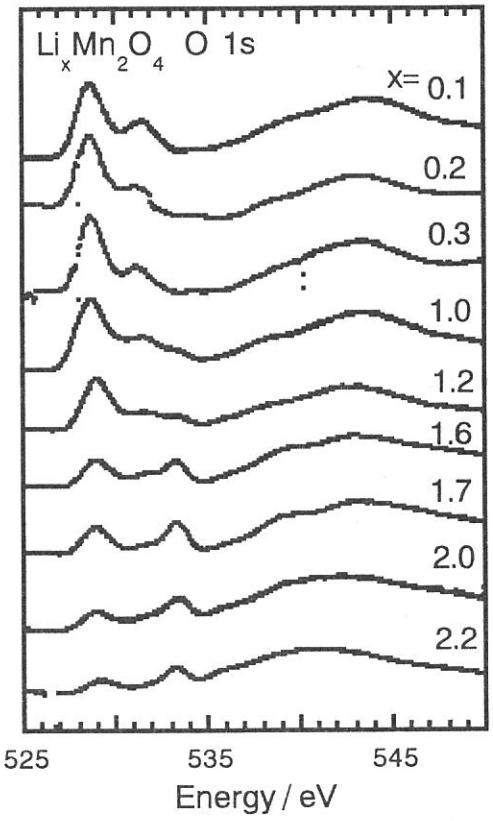

Fig.4 O 1s absorption spectra of $Li_xMn_2O_4$, the value of x is indicated in the figure.

REFERENCES

1) T. Ohzuku, M. Kitagawa, and T. Hirai, *J. Electrochem. Soc.*, **137**, 769 (1990).

2) K. Kanamura, H. Naito, T. Yao, and Z. Takehara, *J. Material Chem.*, **6**, 33 (1997).

3) T. Yao, Y. Oka, and N. Yamamoto, *J. Mater. Chem.*, **32**, 331 (1992).

4) T. Yao, T. Ito, and T. Kokubo, *J. Materials Research*, **10**, 1079 (1995).

5) S.K. Mishra and G. Cedar, *Physical Review B*, **45**, 1612 (1999).

6) M.K. Aydinol and G. Cedar, *J. Electrochem. Soc.*, **144**, 3832 (1997).

(BL8B1)

Nitrogen *K*-edge Absorption of AlInN

Kazutoshi FUKUI, Akio YAMAMOTO [1], Satoru TANAKA [2,3], Yoshinobu AOYAGI [3],
Shigeo YAMAGUCHI [4], Hiroshi AMANO [4,5] and Isamu AKASAKI [4,5]
Institute for Molecular Science, Okazaki 444-8585, Japan
Fax +81-564-54-7079, fukui@ims.ac.jp
[1] *Faculty of Engineering, Fukui University, Fukui 910-8507, Japan*
[2] *Research Institute for Electronic Science, Hokkaido University, Sapporo 060-0812, Japan*
[3] *Institute of Physical and Chemical Research (RIKEN), Wako 351-0198, Japan*
[4] *High-Tech Research Center, Meijo University, Nagoya 468-8502, Japan*
[5] *Department of Materials Science and Technology, Meijo University, Nagoya 468-8502, Japan*

The soft X-ray absorption (SXA) around nitrogen *K*-edge (N-*K*) have been measured to investigate the electronic structure of the wurzite III – V nitrides, especially the structure of the unoccupied states. The N-*K* absorption spectra of III – V nitrides near the N *K*-edge in principle represent the partial density of the final states with *p* symmetry according to the selection rule. Since the core levels are strictly localized in space, the N-*K* absorption spectrum gives us the site-specific information. The N-*K* absorption spectrum also gives us the information about the final states symmetry p_{xy} and p_z, because the incidence soft X-ray light is linearly polarized. In this report, we represent the first results of N-*K* SXA spectra of wurtzite $Al_{1-x}In_xN$ (x= 0, 0.53, 0.78, 1).

The experiments were carried out at BL8B1. Resolution power under the experimental conditions was about 0.5 eV at 400 eV. The soft X-ray absorption measurement was performed by using the total photoelectron yield (TY) method. Thin films were made by the MOCVD method at RIKEN on SiC substrates (x = 0), at Fukui University on GaAs(111) surface (x = 1) and at Meijo University (x = 0.53, 0.78) on α-Al_2O_3 substrates. All films were cleaned with organic solvents just before the installation in the vacuum chamber. No specific surface cleaning of the samples was performed in the vacuum chamber. The TY measurements were carried out at room temperature in the range of 10^{-9} Torr. Sample holder was able to rotate in the vacuum chamber for the angular dependent measurement. The incidence angle θ is defined as the angle between the incident light and the normal axis of the sample surface, i.e., c-axis. The incidence angle dependent SXA measurements were performed under the *p*-polarization configuration which means **E** parallel to *c*-axis at $\theta \sim 90^{\circ}$, where **E** was the electric field of the incident light.

Figure 1 shows the N-*K* absorption spectra of $Al_{1-x}In_xN$ (x= 0, 0.53, 0.78, 1). The energy scale is relative to the threshold energy corresponds to the conduction band minimum. The intensity is normalized at the maximum peak in each spectrum. The spectra features of AlN (x = 0) and InN (x = 1) are good agreement with the previous works [1-3]. The spectrum feature shows the structure-less spectra of x = 0.78 and, in particular, x = 0.53. Figure 2 shows the N-*K* absorption of $Al_{0.78}In_{0.22}N$ as

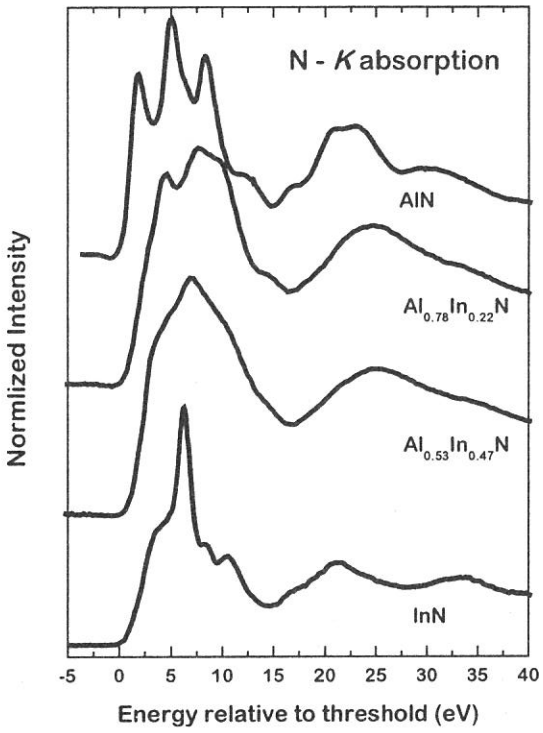

Fig.1 N-K absorption spectra of AlInN. The energy scale is relative to the threshold energy.

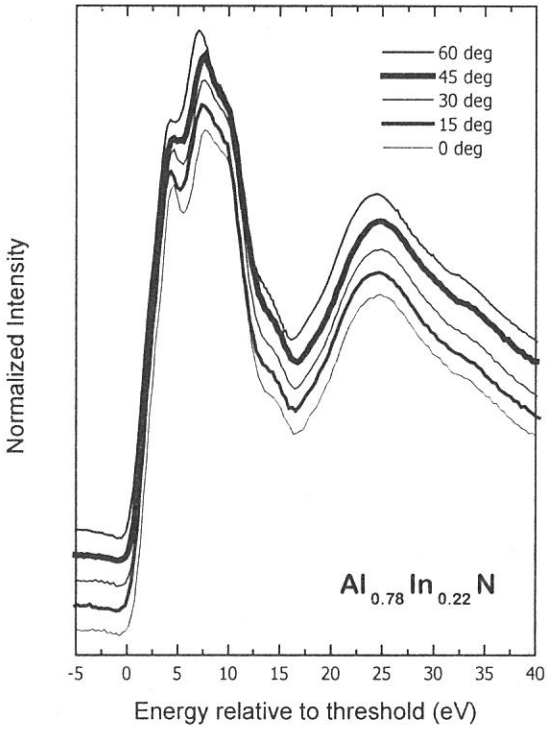

Fig.2 N-K absorption spectra of $Al_{0.78}In_{0.22}N$ as function of angle which is defined as the angles between the incident light and the normal to the sample surface (c–axis).

function of angle θ. All spectra are normalized at the peaks around 7.5 eV. The clear θ dependence can be seen at the lowest peaks and the higher energy side of the maximum peaks. These types of angular dependence are seen in $Al_{1-x}Ga_xN$ and $In_{1-x}Ga_xN$ [2,4]. However, in the spectra of $x = 0.53$ such θ dependence are not found. Both this result and the structure-less feature in Fig. 1 may correspond to the X-ray diffraction results which suggest the c-axis fluctuations of $x = 0.78$ and $x = 0.53$ samples are about 3 and 10 times larger than those of the typical $Al_{1-x}Ga_xN$ samples, respectively.

References

[1] L.-C. Duda, C. B. Stagarescu, J. Downes, K. E. Smith, D. Korakakis, T. D. Moustakas, J. Guo, J. Nordgren, Phys Rev. B **58** (1998) 1928.

[2] K. Fukui, M. Ichikawa, A. Yamamoto and M. Kamada, Solid State Electronics **41** (1997) 299.

[3] K. Fukui, R. Hirai, A. Yamamoto, S. Naoe and S. Tanaka, Jpn. J. Appl. Phys. **38** (1999) Suppl. 38-1, pp. 538.

[4] K. Fukui, R. Hirai and A. Yamamoto, UVSOR Activity Report 1998, 1999, p. 214.

(BL8B2)

Intramolecular Energy-Band Dispersion in Oriented Thin Films of n-$CF_3(CF_2)_{22}CF_3$ Observed by Angle-Resolved UV Photoemission

D. Yoshimura,[a] T. Miyamae,[b] S. Hasegawa,[b] H. Ishii,[a] N. Ueno,[c] and K. Seki [a,d]

a) Department of Chemistry, Graduate School of Science, Nagoya Univ., Chikusa-ku, Nagoya 464-8602 , Japan

b) Institute for Molecular Science, Myodaiji, Okazaki 444-8585, Japan

c) Department of Materials Technology, Faculty of Engineering, Chiba Univ., Inage-ku, Chiba 263-8522, Japan

d) Research Center for Materials Science, Nagoya University, Chikusa-ku, Nagoya 464-8602, Japan

Poly(tetrafluoroethylene) (PTFE) $(CF_2)_n$ is one of the most fundamental polymers, which is the perfluorinated analogue of polyethylene $(CH_2)_n$ with a simple repeating CF_2 unit. PTFE has been widely used for chemical, medical, and high-performance electronic applications due to its excellent chemical stability, low dielectric constant, small dielectric loss, low surface energy, and excellent charge-storage capability. Many of the above mentioned interesting chemical and physical properties of PTFE are related to its valence electronic structures, and its elucidation is important from the viewpoints of both basic science and practical applications.

The electronic structures of PTFE and its oligomers have been studied both experimentally and theoretically. The use of oligomers is based on the theoretical and experimental findings that oligomers more than ten repeating units have very similar electronic structures with infinite polymers. An interesting aspect of such calculations is that a chain in an extended ordered form can be regarded as a one-dimensional crystal, and we can expect the formation of intramolecular one-dimensional bands with intramolecular energy band dispersion ($E = E(\boldsymbol{k})$) relation, where $\boldsymbol{k}$ is the wavevector along the chain. Many calculations for a PTFE chain have indicated large widths of the bands of the order of 5 eV due to the strong interatomic covalent bond within the chain. Unfortunately, however, there were no experimental results to be compared with such calculated intramolecular energy band dispersion relation besides the indirect information of DOS.

In the present work, we report on ARUPS studies of oriented thin films of perfluorotetracosane n-$C_{24}F_{50}$ (PFT), an oligomer of PTFE, prepared by in-situ vacuum evaporation. Thin PFT films showed drastic spectral changes depending on various experimental parameters. In particular, from the $h\nu$ dependence of the normal emission spectra we could successfully determine the intramolecular energy-band dispersion.

ARUPS measurements were carried out at the beamline 8B2 of the UVSOR facility at Institute for Molecular Science. The sample of PFT supplied from Aldrich was used without further purification. Thin films of PFT were prepared by vacuum evaporation at room temperature onto n-doped Si(100) substrates. The pressure during the evaporation was about 4×10^{-9} Torr. Before introducing into the chamber, the substrates were rinsed by acetone for 10 min. The thickness of PFT was about 10 nm as monitored by a quartz oscillator, and the deposition rate was about 0.5 nm/min. For PFT, X-ray diffraction,[1] NEXAFS,[1] and VUV absorption measurements revealed that the molecules in evaporated films prepared in a similar way are well oriented with their long axes vertical to the substrate surface.

In order to minimize the radiation damage, the incident light intensity was reduced less than 50 pA, and the sampling position of specimen was changed after several runs. The absence of the damage effect was confirmed by remeasuring spectra under fixed experimental parameters.

The $h\nu$ dependence of the spectra of the PFT thin film for photoelectrons emitted normal to the surface at $22 \leq h\nu \leq 60$ eV is shown in Fig. 1. The emission intensities of these spectra are normalized by the photon flux of the incident photon energy. The main features show continuous and significant changes in both peak positions and intensities. In the upper part of the valence bands extending from 10.5 to 14.5 eV, the position of peak A slightly changes at around $h\nu = 30$ eV, and shifts towards higher binding energies with increasing photon energy for $h\nu \geq 34$ eV. Another feature B is observed for $h\nu \leq 28$ eV. In the F_{2p} region at 14.5 – 18 eV (peak C), drastic changes in the intensity are seen.

We attribute the peak shifts to the intramolecular energy-band dispersion. The dispersion relation can be determined according to the method reported in ref. 2 by assuming that the photoexcitation are dominated by direct transitions, and the final state follow the dispersion relation of a nearly free-electron-like parabola. Considering the initial state broadening of $\boldsymbol{k}$ (or relaxation of $\boldsymbol{k}$-conversation rule) due to the small number of repeating units, we can regard the PFT molecules have sufficient number of repeating units for mapping the energy band structure.[3] In Fig. 2, we display the experimentally derived band structure obtained by the procedure as described in ref. 2. In order to map out the energy-band dispersion, we took the second derivative of the ARUPS spectra after smoothing for specifying the energies of the spectral features. We assumed the length of repeating unit as 2.6 Å. In this figure, the bright regions correspond to the bands. For comparison, we also show the results of an ab initio band calculation for a PTFE chain in planar-zigzag geometry by Seki et al.[4] The energy-scale of the calculated band structure was 0.95 times contracted and shifted 1.8 eV to the higher binding energy side. We also compare another calculated band structures, but good correspondence is not obtained at the whole

energy region. The correspondence between the observed and calculated band structure is fairly good, although there are differences in details. In particular, the detailed shape of the topmost band is quite different.

There are several possible origins of such difference between the observed and calculated band structures. First, the calculation assumed a planar molecular structure, while the actual PTFE chain has a helical structure.[5] Energy band calculations for PTFE in helical- and planar-zigzag- configurations indicate dihedral-angle difference in the calculated DOS. Especially, the shape of the topmost band shows the dihedral-angle dependence, although the shapes of the topmost band in these calculations with helical form are still quite different from the observed one. The second is that the accurate band structure may not be directly observed because low $h\nu$ is used for the excitation. In the case of ARUPS measurements of polyethylene, the top portion of the valence bands is not observed when low $h\nu$ light was used for the excitation although the reason is unknown.[2] Thirdly, the interference pattern of electron waves leading to the $\boldsymbol{k}$ conservation rule may be different between the helical structure with a long repeating unit of ~ 13 carbons and that in the assumed planar-zigzag structure with a repeating period of only 2 carbon atoms.

Although no satisfactory quantitative explanation is available for the observed difference at present, these points may be clarified by better calculations. In particular, the calculation of photoemission intensity by using independent-atomic-center (IAC) and single-scattering approximations combined with molecular orbital (MO) calculations have been successfully applied to the analysis of the photoelectron angular distribution for oriented organic thin films and the energy-band dispersion of solid surface.[6,7] We are currently performing such calculations.

REFERENCES [1] K. Nagayama, R. Mitsumoto, T. Araki, Y. Ouchi, and K. Seki, Physica B **208/209**, 414 (1995).
[2] K. Seki, N. Ueno, U. O. Karlsson, R. Engelhardt, and E. E. Koch, Chem. Phys. **105**, 247 (1986).
[3] T. Miyamae, S. Hasegawa, D. Yoshimura, H. Ishii, N. Ueno, and K. Seki, J. Chem. Phys., in press.
[4] K. Seki, H. Tanaka, T. Ohta, Y. Aoki, A. Imamura, H. Fujimoto, H. Yamamoto, and H. Inokuchi, Phys. Scripta **41**, 167 (1990).
[5] C. W. Bunn and E. R. Howells, Nature **174**, 549 (1954).
[6] N. Ueno, A. Kitamura, K. K. Okudaira, T. Miyamae, S. Hasegawa, H. Ishii, H. Inokuchi, T. Fujikawa, T. Miyazaki, and K. Seki, J. Chem. Phys. **107**, 2079 (1997).
[7] D. Yoshimura, H. Ishii, Y. Ouchi, E. Ito, T. Miyamae, S. Hasegawa, K. K. Okudaira, N. Ueno, and K. Seki, Phys. Rev B **60**, 9046 (1999)

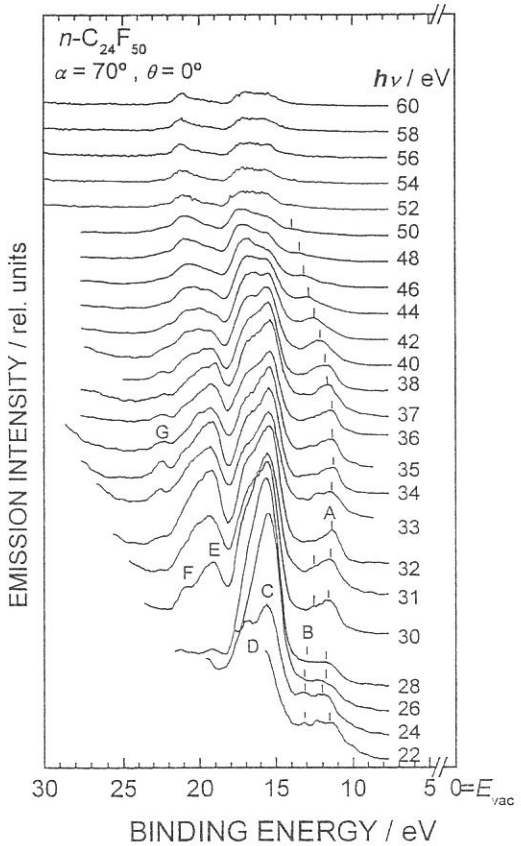

Fig. 1. $h\nu$-dependence of the normal-emission spectra of PFT thin films for $\alpha = 70°$.

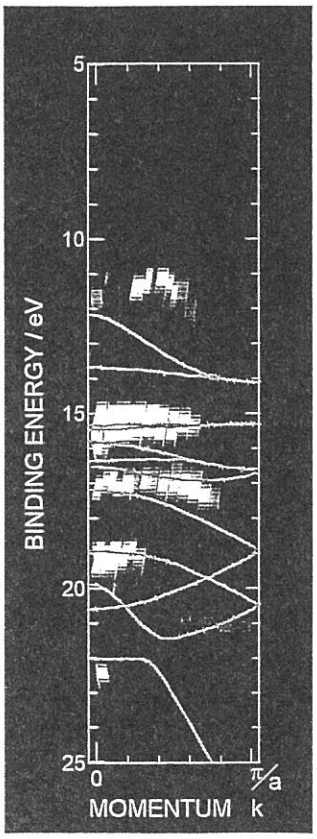

Fig. 2. Experimentally determined band structure for PFT.

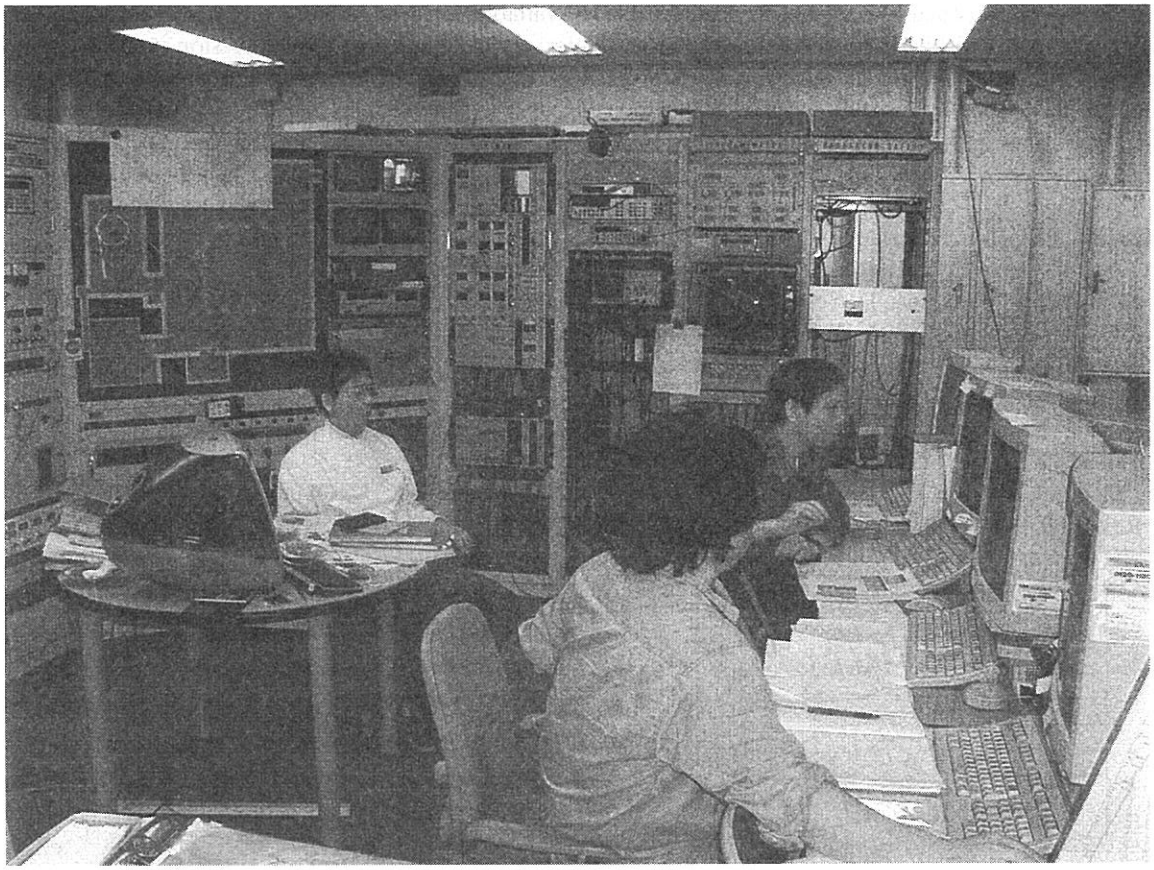

Injection is started!!